A network of transcriptional repressors modulates auxin responses.

Jekaterina Truskina, Jingyi Han, Elina Chrysanthou, Carlos Galvan-Ampudia, Stéphanie Lainé, Geraldine Brunoud, Julien Macé, Simon Bellows, Jonathan Legrand, Anne-Maarit Bågman, et al.

A network of transcriptional repressors modulates auxin responses

Jekaterina Truskina[1,2], Jingyi Han[2*], Elina Chrysanthou[2*], Carlos Galvan-Ampudia[1], Stéphanie Lainé[1], Géraldine Brunoud[1], Julien Macé[1], Simon Bellows[3], Jonathan Legrand[1], Anne-Maarit Bågman[4], Margot E. Smit[4], Ondřej Smetana[5], Arnaud Stigliani[6], Silvana Porco[2], Malcolm J. Bennett[2], Ari Pekka Mähönen[5], François Parcy[6], Etienne Farcot[2,3], Francois Roudier[1], Siobhan M. Brady[4], Anthony Bishopp[2†], Teva Vernoux[1†]

[1] Laboratoire Reproduction et Développement des Plantes, Univ Lyon, ENS de Lyon, UCB Lyon 1, CNRS, INRAE, F-69342, Lyon, France

[2] Centre for Integrative Plant Biology and School of Biosciences, University of Nottingham, Sutton Bonington Campus, Loughborough, LE12 5RD, UK.

[3] School of Mathematical Sciences, University of Nottingham, Nottingham, NG7 2RD, UK

[4] Department of Plant Biology and Genome Center, University of California Davis, Davis, CA, USA

[5] Institute of Biotechnology (HiLIFE) /Faculty of Biological and Environmental Sciences, University of Helsinki, Helsinki 00014, Finland

[6] Univ Grenoble Alpes, CNRS, CEA, INRAE, IRIG-DBSCI-LPCV, Grenoble, France

[*]These authors contributed equally

[†]To whom correspondence should be addressed: T.V. (teva.vernoux@ens-lyon.fr) or A.B. (Anthony.Bishopp@nottingham.ac.uk)

Alongside spatio-temporal distribution of developmental signals themselves, the regulation of signalling capacity plays a pivotal role in setting developmental responses in both plants and animals (1). The hormone auxin is a key signal for plant growth and development that acts through the AUXIN RESPONSE FACTOR (ARF) transcription factors (2-4). Subsets of ARFs, the conserved Class A ARFs (abbreviated ARF^{ClassA}) (5), are transcriptional activators of auxin-responsive target genes, and are essential for regulating auxin signalling throughout the plant lifecycle (2,3). While ARF^{ClassA} show tissue-specific expression patterns, it is unknown how their expression is regulated. By investigating chromatin modifications and accessibility, we show that loci encoding ARF^{ClassA} are constitutively open for transcription. Using a yeast one-hybrid (Y1H) approach, we identify transcriptional regulators of *ARF^{ClassA}* activator genes from *Arabidopsis thaliana,* and demonstrate that each *ARF^{ClassA}* is controlled by specific sets of transcriptional regulators. Transient transformation assays and expression analyses in mutants reveal that the majority of these regulators act as repressors of *ARF^{ClassA}* transcription *in planta*. Taken together these observations support a scenario whereby the default configuration of open chromatin enables a network of transcriptional repressors to regulate expression level of ARF^{ClassA} and modulate auxin signalling output throughout development.

Transcriptional regulation of *ARF^{ClassA}*

Amongst the 23 Arabidopsis ARFs, ARF5, 6, 7, 8 and 19 are ARF^{ClassA} activators of transcription (3) and are key regulators of both embryonic and post-embryonic development (6-12). In the stem cell niches driving post-embryonic plant development, the root and shoot apical meristems (RAM and SAM) (6), tissue-specific variation of *ARF^{ClassA}* expression (Fig.1a,b), is thought to be a key determinant of the diversity of auxin responses (14, 15). ARF^{ClassA} are encoded by genes with 11-14 introns and the first intron of ARF7 and 19 is around 3 times

bigger than the other introns. We tested the role of upstream sequences in determining *ARF*^{ClassA} expression by comparing patterns in meristems from transcriptional reporter lines (Fig.1a,b, Extended Fig.1a-j) using either sequences 3-5 kb 5' of the ATG and 3' up to the end of the first intron for ARF6, 7 and 19 or the 5' sequences alone (designated respectively *pARF* and *pARF*$^{-intron}$). A difference between the two reporters was only seen for *ARF7* (Fig.1a,b, Extended Fig.1c,h). Only the *ARF7* transcriptional reporter including the first intron showed a strong expression in the RAM (Fig.1b). The 3' sequence thus contains regulatory information required for *ARF7* expression in the root. Comparison with patterns of *ARF*^{ClassA} reporters with shorter 2 kb promoters (Extended Fig.1k-o, (14)) and with patterns observed with RNA *in situ* hybridization (Extended Fig.1p-r; (15,16)) further showed that sequences upstream of the first 2 kb 5' of the ATG are necessary for regulation of *ARF*^{ClassA} expression.

Chromatin status of *ARF*^{ClassA} loci

Specific *ARF*^{ClassA} expression patterns could be due to tissue-specific differences in chromatin accessibility of *ARF*^{ClassA} loci. We analysed chromatin status of each *ARF*^{ClassA} locus by scoring the presence of H3K27me3 and H3K4me3 chromatin modifications, as they are implicated in repressing and promoting gene expression, respectively (17). Meta-analysis of published datasets covering a whole range of tissues and developmental stages shows H3K27me3 is largely absent from all *ARF*^{ClassA} loci while H3K4me3 is detected at these loci (Fig.1c, Extended Data Fig.2a-c, Supplementary Table 1). *ARF*^{ClassA} loci are also characterized by accessible regulatory regions in the majority of tissues (Fig.1c, Extended Data Fig.2d, Supplementary Table 1). These properties suggest a chromatin configuration of *ARF*^{ClassA} loci allowing them to be actively transcribed throughout different tissues and developmental stages; this indicates *ARF*^{ClassA} specific spatial expression does not result primarily from alternate chromatin states with contrasting accessibility.

Repressors as regulators of *ARF*^{ClassA}

Specific spatiotemporal transcription of *ARF*^{ClassA} loci could then arise from regulatory networks made up of transcription factors (TFs). To identify TFs that could regulate *ARF*^{ClassA} transcription, we used a semi-automated enhanced Y1H (eY1H) assay with baits consisting of promoter sequences identical to those from the transcriptional reporter lines described above. The assay yielded 42 novel putative transcriptional regulators of *ARF*^{ClassA} (Fig.2, Extended Fig.3a,b, Supplementary Table 2). This candidate gene regulatory network revealed that individual *ARF*^{ClassA} loci are likely regulated by specific sets of TFs, with only 4 TFs identified that bind multiple *ARF*^{ClassA} sequences. Based on the expression of these TFs, the network may contain proteins that mediate either root- or shoot-specific responses (Extended Data Fig.3c). The majority of the TFs from the network are involved in development, but many putative regulators of *ARF8* are associated with biotic and abiotic stress (Extended Data Fig.3d, Supplementary Table 2). ARF8 may therefore act as an environmental hub to mediate auxin responsiveness, and indeed it has been shown to play a role in biotic and abiotic stresses (18, 19).

To validate this regulatory network, we searched *ARF*^{ClassA} promoters for the presence of binding sites for the eY1H-identified TFs. We could predict the presence of many of these TF binding sites within the ARF promoters and show that a small proportion of the inferred bindings are confirmed experimentally (Extended Data Fig.3e-g, Supplementary Table 3, (20, 21)). We next systematically tested the regulatory activity of each TF through transient expression analysis using either TFs alone or a fusion of TFs to the VP16 transactivation domain (Extended Data Fig.4a,b, Supplementary Table 4). 34 out of 42 (81%) TFs induced in a significant change in expression of its *ARF*^{ClassA} target(s), corresponding to a decrease in *ARF*^{ClassA} mRNA level in 32 out of 34 of cases (94%; 76% of total number of TFs) (Fig.2, Supplementary Table 4, Supplementary Note 1). Repression of *ARF*^{ClassA} transcription was frequently observed both for TFs alone and TF-VP16 fusions, indicating a strong repressive

activity (Extended data Fig.4c,d, Supplementary Table 4). Taken together, our data reveal a functional regulatory network controlling *ARF*^{ClassA} transcription and demonstrate that *ARF*^{ClassA} transcription is regulated by TF-mediated repression.

Expression of *ARF*^{ClassA} regulators

If *ARF*^{ClassA} expression is controlled by tissue-specific transcriptional repression, we would expect many of these repressors to have expression patterns complementary to their target *ARF*. To test the complementarity of expression with a high spatial resolution, we generated transcriptional reporters for 6 TFs and investigated them in 7 combinations with *ARF*^{ClassA} reporters in both RAM and SAM (Fig.3a,b, Extended Fig.5). We observed complementary expression patterns in 5 out of 7 cases analysed in the root (Fig.3b, Extended Fig.5a,b). In the shoot we looked at 2 combinations involving *WRKY11* and *At2g26940*. We detected *WRKY11* only in L2/3 layers with its target *ARF8* expressed specifically in the L1 layer (Fig.3a). In the SAM, *At2g26940* was expressed weakly in the centre, where *ARF19* shows low expression in flower primordia, therefore this TF was present in different cells than *ARF19* (Extended data Fig.5c). Hence, repressors and their target ARFs have mostly complementary expression patterns in both shoot and root tissues, although co-localisation of repressors and their target occurs in some cells as observed with other TFs (22, 23).

Mutants in *ARF*^{ClassA} regulators

To further test the significance of our results *in planta*, we characterised mutants of 24 TFs from the regulatory network representing regulators of all five ARF^{ClassA} members (Supplementary Table 5). We measured the expression of target *ARF*^{ClassA} using qRT-PCR in whole root and shoot tissues (Extended Data Fig.6, Supplementary Table 6). We detected changes in the expression of target *ARF*^{ClassA} genes identified in our network in 11 out of 24 mutants (46%). Four showed up-regulation of their target ARFs, compatible with a repressive

activity. The other seven, six of which are ARF8 regulators, showed a down-regulation of their target ARF. In the case of ARF8, this could be explained by complex, non-linear regulations of ARF8 expression by multiple TFs. Indeed, the ARF8 regulators tested are themselves directly or indirectly regulated transcriptionally by ARF8 both negatively and positively, thus establishing a network structure that could result in *ARF8* upregulation in mutants (Extended Data Fig.7, Supplementary Note 2). The low-sensitivity of expression analysis on whole tissues could also explain our results. This prompted us to determine at higher spatial definition how TF mutations affect ARF^{ClassA} expression. We crossed *pARF7::mVENUS* and *pARF19::mVENUS* transcriptional reporters into a number of TF mutants. For *crf10* and *wrky38* in which we had not seen changes in *ARF7* mRNA levels using qRT-PCR, we observed a significant increase in expression and an expansion of *pARF7::mVENUS* expression pattern in the RAM (Extended Data Fig.8a,b,h). For *nf-yb13*, in agreement with qRT-PCR results, we observed enhanced expression of *pARF7::mVENUS* in the RAM (Extended Data Fig.8c,h). However, we saw no changes in the root for 3 mutants in which we analysed *pARF19::mVENUS* expression (Extended Data Fig.8d-f,h). In *nf-yb13* SAM, *pARF7*-driven fluorescence was identical to wild-type in the L1 layer but elevated in L2/3, indicating a change in the spatial pattern of *pARF7* (Fig.3c,d, Extended Data Fig.8h). We also detected expression pattern changes for *pARF7::mVENUS* in *wrky38* SAMs (Extended Data Fig.8g,h). In addition, inducible constitutive overexpression of AL3 and CRF10 in the *pARF7::mVENUS* background triggered a decrease in mVENUS signal (Extended Data Fig.8i,j). These results confirm *in planta* that four TFs are repressors and provide examples of how repressors shape the expression level or pattern of an ARF^{ClassA}.

To investigate the functional role of this network, the 24 TF mutants were scored for defects in auxin-regulated root processes (Fig.3e, Extended Data Fig.9, Supplementary Table 7). Whilst none of these mutants had previously been implicated in auxin-dependent responses, 58% (14/24) of them showed a defect in root length response to auxin treatment, whilst 29% (7/24)

were affected in gravitropism. 64 % (9/14) of the mutants affected in root length response to exogenous auxin exhibited an enhanced response and all mutants affected in gravitropism had a faster response. Thus, for both traits, a majority of the TF mutants showing defective auxin response have opposite effects to those observed for mutants in loci known to promote auxin signalling (12, 24), consistent with a repressive role. We selected two high auxin-responsive genes in the root, *IAA13* and *IAA19*, and tested their expression in the mutants. Despite only mutating one transcriptional regulator at a time, we found a small but significant increase in the expression of *IAA19* in the roots of 7 mutants (~28%) with 2 of these also showing elevated levels of *IAA13*. A reduction in either *IAA13* or *IAA19* was observed in a further 3 mutants (~12%) (Supplementary Table 8). A significant number of the mutants also showed shoot phenotypes, further demonstrating an important role in development (Extended Data Fig.10, Supplementary Table 9). Taken together, our results support a negative regulation of auxin responses by the corresponding TFs. Mutation of single genes in the ARF^{ClassA} regulatory network can significantly affect auxin-dependent developmental responses, further demonstrating the functional importance of individual nodes of this network.

Discussion

Despite a general role of Polycomb-mediated gene repression in tissue-specific expression (25), the general absence of H3K27me3 at ARF^{ClassA} loci indicates that their regulation does not rely on this epigenetic mechanism. This may be because such a system would not allow for rapid changes in signalling output. Instead, our data suggest a regulatory system based on the use of transcriptional repressors that, in combination with post-translational modifications of ARF^{ClassA} (26, 27), modulates expression of constitutively active loci and constantly adjust auxin responsiveness during development. Other transcriptional regulation networks defined in eukaryotes involve both transcriptional activators and repressors (28). Instead, the network we characterise resembles the early scenario proposed by Jacob and Monod (29) for transcriptional

regulation by repressors only, indicating that there may be a place for the concept of controlling the expression of key developmental regulators via transcriptional repression.

References

1. Sagner, A. & Briscoe, J. Morphogen interpretation: concentration, time, competence, and signaling dynamics. *Wiley Interdiscip Rev Dev Biol* **6,** (2017).

2. Leyser, O. Auxin Signaling. *Plant Physiol.* **176,** 465–479 (2018).

3. Tiwari, S. B., Hagen, G. & Guilfoyle, T. The roles of auxin response factor domains in auxin-responsive transcription. *Plant Cell* **15,** 533–543 (2003).

4. Petrásek, J. & Friml, J. Auxin transport routes in plant development. *Development* **136**, 2675–2688 (2009).

5. Finet, C., Berne-Dedieu, A., Scutt, C. P. & Marlétaz, F. Evolution of the ARF gene family in land plants: old domains, new tricks. *Mol. Biol. Evol.* **30,** 45–56 (2013).

6. Krogan, N. T., Marcos, D., Weiner, A. I. & Berleth, T. The auxin response factor MONOPTEROS controls meristem function and organogenesis in both the shoot and root through the direct regulation of PIN genes. *New Phytol.* **212,** 42–50 (2016).

7. Berleth, T. & Jurgens, G. The role of the monopteros gene in organising the basal body region of the Arabidopsis embryo. *Development* **118,** 575–587 (1993).

8. Przemeck, G. K., Mattsson, J., Hardtke, C. S., Sung, Z. R. & Berleth, T. Studies on the role of the Arabidopsis gene MONOPTEROS in vascular development and plant cell axialization. *Planta* **200,** 229–237 (1996).

9. Schlereth, A. *et al.* MONOPTEROS controls embryonic root initiation by regulating a mobile transcription factor. *Nature* **464,** 913–916 (2010).

10. Nagpal, P. *et al.* Auxin response factors ARF6 and ARF8 promote jasmonic acid production and flower maturation. *Development* **132,** 4107–4118 (2005).

11. Gutierrez, L. *et al.* Phenotypic plasticity of adventitious rooting in Arabidopsis is controlled by complex regulation of AUXIN RESPONSE FACTOR transcripts and microRNA abundance. *Plant Cell* **21,** 3119–3132 (2009).

12. Okushima, Y. *et al.* Functional genomic analysis of the AUXIN RESPONSE FACTOR gene family members in Arabidopsis thaliana: unique and overlapping functions of ARF7 and ARF19. *Plant Cell* **17,** 444–463 (2005).

13. Harper, R. M. *et al.* The NPH4 locus encodes the auxin response factor ARF7, a conditional regulator of differential growth in aerial Arabidopsis tissue. *Plant Cell* **12,** 757–770 (2000).

14. Rademacher, E. H. *et al.* A cellular expression map of the Arabidopsis AUXIN RESPONSE FACTOR gene family. *Plant J.* **68,** 597–606 (2011).

15. Vernoux, T. *et al.* The auxin signalling network translates dynamic input into robust patterning at the shoot apex. *Mol. Syst. Biol.* **7,** 508 (2011).

16. Hardtke, C. S. & Berleth, T. The Arabidopsis gene MONOPTEROS encodes a transcription factor mediating embryo axis formation and vascular development. *EMBO J* **17**, 1405–1411 (1998).

17. Roudier, F. *et al.* Integrative epigenomic mapping defines four main chromatin states in Arabidopsis. *EMBO J.* **30,** 1928–1938 (2011).

18. Gifford, M. L., Dean, A., Gutierrez, R. A., Coruzzi, G. M. & Birnbaum, K. D. Cell-specific nitrogen responses mediate developmental plasticity. *Proc. Natl. Acad. Sci. U.S.A.* **105**, 803–808 (2008).

19. Jay, F. *et al.* Misregulation of AUXIN RESPONSE FACTOR 8 Underlies the Developmental Abnormalities Caused by Three Distinct Viral Silencing Suppressors in Arabidopsis. *PLOS Pathogens* **7**, e1002035 (2011).

20. O'Malley, R. C. *et al.* Cistrome and Epicistrome Features Shape the Regulatory DNA Landscape. *Cell* **165,** 1280–1292 (2016).

21. Ma, Y. *et al.* WUSCHEL acts as an auxin response rheostat to maintain apical stem cells in Arabidopsis. *Nature Communications* **10**, 5093 (2019).

22. Zhao, Z. *et al.* Hormonal control of the shoot stem-cell niche. *Nature* **465**, 1089–1092 (2010).

23. Leibfried, A. *et al.* WUSCHEL controls meristem function by direct regulation of cytokinin-inducible response regulators. *Nature* **438**, 1172–1175 (2005).

24. Dharmasiri, N. *et al.* Plant development is regulated by a family of auxin receptor F box proteins. *Dev. Cell* **9,** 109–119 (2005).

25. Kim, D.-H. & Sung, S. Polycomb-mediated gene silencing in Arabidopsis thaliana. *Mol. Cells* **37,** 841–850 (2014).

26. Orosa-Puente, B. *et al.* Root branching toward water involves posttranslational modification of transcription factor ARF7. *Science* **362**, 1407–1410 (2018).

27. Cho, H. *et al.* A secreted peptide acts on BIN2-mediated phosphorylation of ARFs to potentiate auxin response during lateral root development. *Nat. Cell Biol.* **16**, 66–76 (2014).

28. Ptashne, M. Repressors. *Current Biology* **17,** R740–R741 (2007).

29. Jacob, F. & Monod, J. Genetic regulatory mechanisms in the synthesis of proteins. *J. Mol. Biol.* **3,** 318–356 (1961).

Figure legends

Fig.1 Tissue specific expression patterns and chromatin landscape of Arabidopsis *ARF*^{ClassA} loci. Expression of *ARF*^{ClassA} in the SAM (a) and RAM (b) reported using long promoters containing sequences 5' and 3' of the ATG (*pARF::mVenus*). For SAM images, orthogonal projections are shown below the relevant panel. Scale bars: 50 µm. Experiments were performed at least 3 times with similar results. (c) Frequency of association of the repressive chromatin marker H3K27me3, active chromatin marker H3K4me3 and chromatin accessibility with the *ARF*^{ClassA} loci across all available datasets.

Fig.2 *ARF*^{ClassA} transcription is regulated by repressors

eY1H promoter-transcription factor interaction network for *ARF*^{ClassA}. Interactions between *ARF*^{ClassA} promoters and the regulatory TFs were tested using transient protoplast assays. Green boxes correspond to the *ARF*^{ClassA}. Solid lines: confirmed repression; dashed lines: confirmed transcriptional activity; thin grey lines: interaction not confirmed. TFs for which binding has been shown by DAP-seq or Chip-seq are shown with a light red background (see Supplementary Table 3).

Fig.3 Expression levels and patterns of *ARF*^{ClassA} are altered when upstream transcription factors are modulated. (a,b) *ARF8* and *WRKY11* show complementary expression patterns in the SAM (a) and RAM (b). For SAM images, orthogonal projections are shown at the bottom of (a). (c,d) *pARF7*-driven patterns are altered in the SAM of *nf-yb13* mutant. Experiments were done two time (a-d). Scale bars: 40 µm (a); 60 µm (b), 45 µm (c and d). (e) Quantification of auxin response in mutant lines. The graph shows percentage change in root elongation for plants grown on 10 µM IAA at 15 days versus plants grown without IAA. All values have been normalised to wild type controls. N of wt/mutant plants + and - IAA (p-values) from left to right: 26/31 and 29/27 (0.002), 24/28 and 28/29 (0.003), 22/31 and 26/23 (0.015), 27/30 and

30/32 (0.03), 30/32 and 29/31 (0.0003), 24/30 and 31/32 (0.61), 31/31 and 29/30 (0.80), 24/31 and 31/32 (0.98), 18/30 and 30/25 (0.72), 30/30 and 31/28 (0.37), 29/30 and 28/27 (0.28), 30/30 and 29/30 (0.07), 29/30 and 31/25 (0.05), 28/28 and 32/30 (0.24), 19/30 and 27/28 (0.19), 22/25 and 29/28 (0.048), 23/27 and 29/32 (0.016), 21/27 and 27/30 (0.003), 28/30 and 31/27 (0.00002), 15/29 and 28/27 (0.004), 24/25 and 31/28 (3e-07), 15/28 and 29/30 (0.002), 28/31 and 29/29 (1e-09) and 28/28 and 27/31 (1e-09). Statistical analyses: two-sided t-test with $p \leq 0.05$ (*) and $p \leq 0.01$ (**) comparing variation in the rate of elongation on IAA against the wt control.

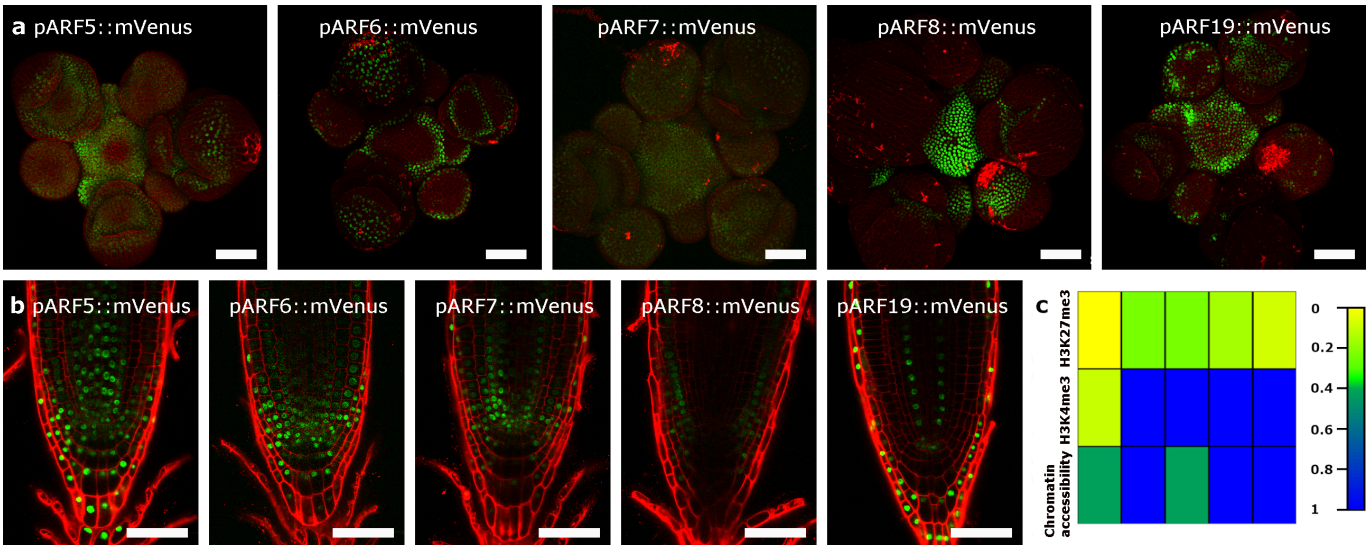
a pARF5::mVenus
pARF6::mVenus
pARF7::mVenus
pARF8::mVenus
pARF19::mVenus
b pARF5::mVenus
pARF6::mVenus
pARF7::mVenus
pARF8::mVenus
pARF19::mVenus
c
H3K27me3
H3K4me3
Chromatin accessibility
0
0.2
0.4
0.6
0.8
1

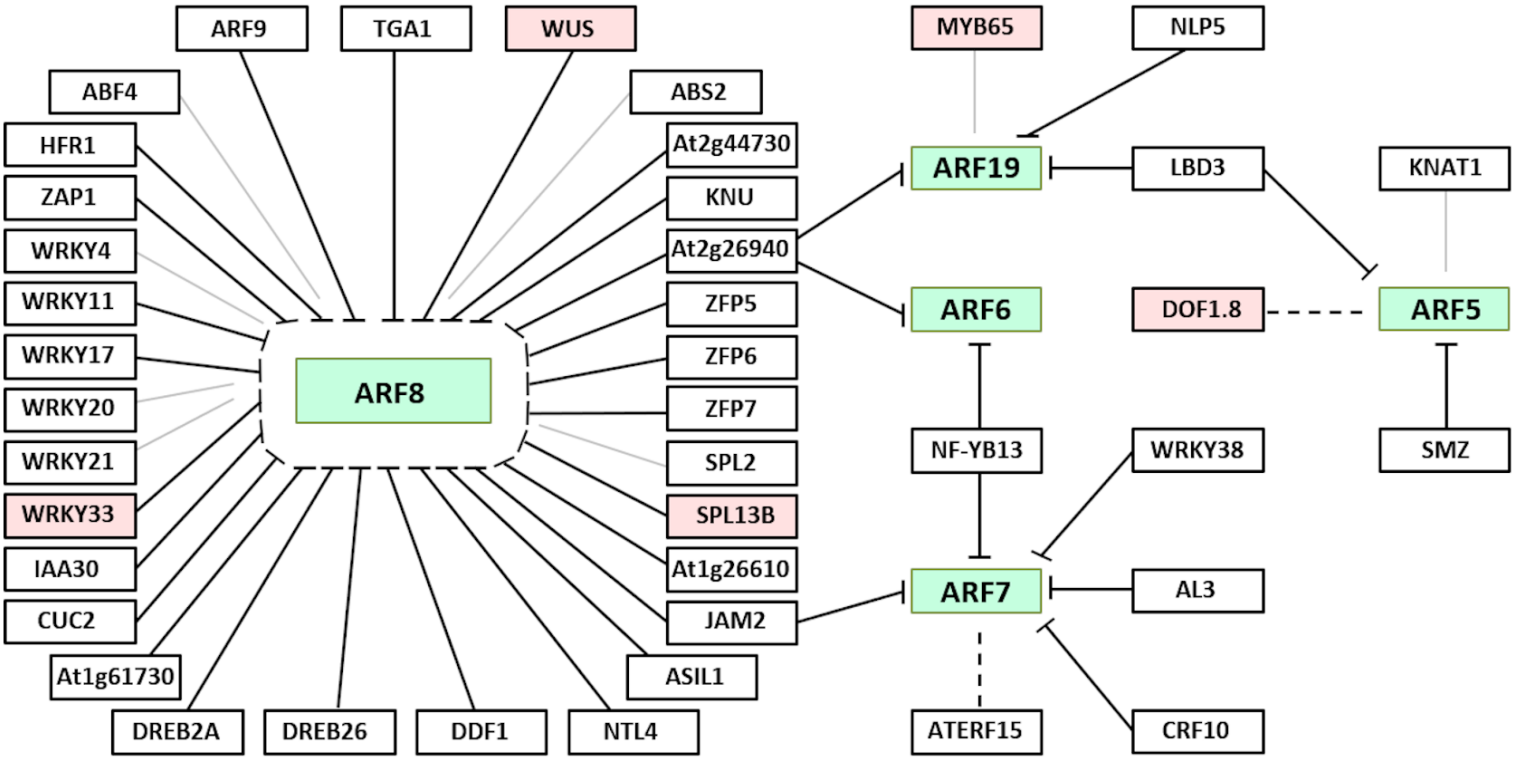
ARF9
TGA1
WUS
ABF4
ABS2
HFR1
At2g44730
ZAP1
KNU
WRKY4
At2g26940
WRKY11
ZFP5
WRKY17
ZFP6
WRKY20
ZFP7
WRKY21
SPL2
WRKY33
SPL13B
IAA30
At1g26610
CUC2
JAM2
At1g61730
ASIL1
DREB2A
DREB26
DDF1
NTL4
ARF8
MYB65
NLP5
ARF19
LBD3
KNAT1
ARF6
DOF1.8
ARF5
NF-YB13
WRKY38
SMZ
ARF7
AL3
ATERF15
CRF10

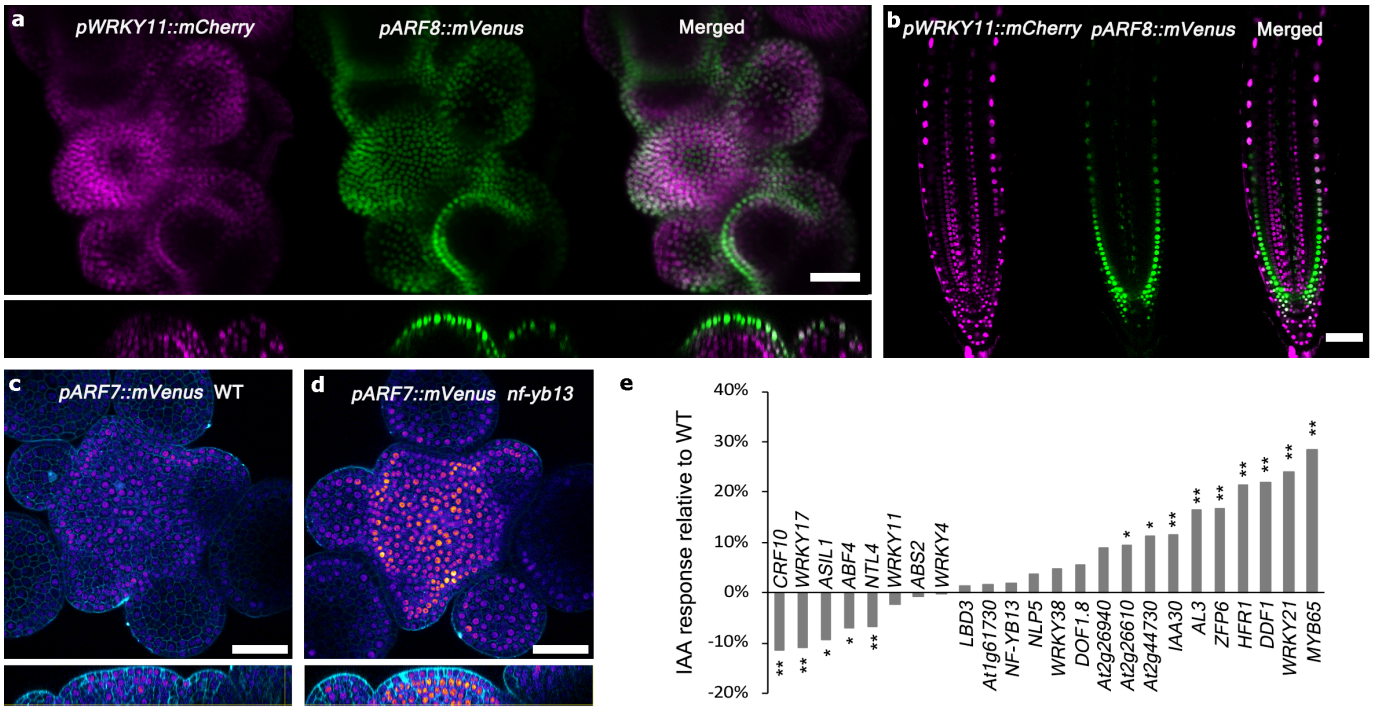
a
pWRKY11::mCherry
pARF8::mVenus
Merged
b
pWRKY11::mCherry
pARF8::mVenus
Merged
c
pARF7::mVenus
WT
d
pARF7::mVenus
nf-yb13
e
IAA response relative to WT
40%
30%
20%
10%
0%
-10%
-20%
CRF10
WRKY17
ASIL1
ABF4
NTL4
WRKY11
ABS2
WRKY4
LBD3
At1g61730
NF-YB13
NLP5
WRKY38
DOF1.8
At2g26940
At2g26610
At2g44730
IAA30
AL3
ZFP6
HFR1
DDF1
WRKY21
MYB65

Methods

Plant material and growth conditions

All transgenic lines were generated in the Col-0 accession. T-DNA insertion mutants in transcription factor coding genes and the *arf8-1* mutant were obtained from NASC. All T-DNA lines were genotyped to confirm that they were homozygous, and qRT-PCR was used to confirm alterations in transcript levels (Supplementary Table 5). The accession numbers of T-DNA lines and further details are listed in Supplementary Table 5.

For root microscopy and *in situ* hybridization of ARF transcriptional reporter lines plants were grown on half-strength Murashige and Skoog (MS) medium supplemented with 1% sucrose and 1% agar in 24h light conditions (microscopy) or 12h light/12h dark conditions (*in situ* hybridization). For shoot microscopy, plants were grown in 8h light/16h dark conditions for 6 weeks and then transferred to 16h light/8h dark conditions for 2 weeks to induce bolting. For the qRT-PCR experiments the seedlings were grown in 24h light conditions on 1/2 MS plates containing 1% sucrose and 1% agar for 7 days. For the root imaging of crosses between ARF transcriptional reporter lines and TF mutants and for the co-expression analysis of ARF transcriptional reporter lines with TF transcriptional reporter lines the plants were grown on 1/2 MS medium supplemented with 0.8% agar in 16h light / 8h dark light. TF overexpression lines were grown for 12h light / 12h dark light on 1/2 MS medium supplemented with 1% agar.

Cloning

Multisite Gateway cloning technology was used to generate ARF transcriptional reporter lines harbouring DNA sequences both upstream and downstream from the start codon. The promoter fragments were amplified by PCR with sequences: *pARF5* -5418 bp to + 134 bp, *pARF6* -3255 bp to +197 bp, *pARF7* -2973 bp to + 374 bp, *pARF8* -5091 bp to + 42 bp, *pARF19* -4906 bp to + 457 bp. For ARF5, 6, 8, and 19 the fragments were inserted into pDONR P4-P1R and recombined with 3x mVenus-N7 pDONR211 (containing triple mVenus coding sequences and

N7 nuclear localization signal), OCS terminator pDONR P2R-P3 (containing the stop codon followed by a octopine synthase terminator) and pK7m34GW (the destination vector containing kanamycin resistance gene for *in planta* selection) to produce pARF-3xmVenusN7 constructs. For ARF7, the fragment was cloned into a pCR8/GW/TOPO and recombined with a nuclear-localized mVenusN7, 35S terminator and pK7m34GW to produce pARF7-mVenusN7 construct. Similarly, the shorter promoter fragments were amplified by PCR based on primers designed at the following locations: *pARF5* -5418 bp to -1 bp, *pARF6* -3255 bp to -1 bp, *pARF7* -2973 bp to -1 bp, *pARF8* -5091 bp to -1 bp, *pARF19* -4906 bp to -1 bp. The fragments were inserted into pDONR P4-P1R and recombined with 3x mVenus-N7 pDONR211, OCS terminator pDONR P2R-P3 and pK7m34GW destination vector to yield pARF-3xmVenusN7 shorter transcriptional reporter lines.

All constructs were transformed into *Agrobacterium tumefaciens* C58pMP90 strain by electroporation and then transformed into Col-0 plants by floral dip method (30).

The ARF promoter sequences screened in the eY1H assay were amplified by PCR and sequenced to confirm absence of mutations. The overall ARF promoters screened correspond in length and content to the ones used in the construction of the transcriptional reporter lines, however the longer promoters were split into two fragments: *pARF5* fragment 1: -2796 bp to + 134 bp, *pARF5* fragment 2: - 5418 bp to -2481 bp, *pARF6*: -3255 bp to +197 bp, *pARF7* -2973 bp to + 374 bp, *pARF8* fragment 1: -2899 bp to + 42 bp, *pARF8* fragment 2: -5091 bp to -2121 bp, *pARF19* fragment 1: -2399 bp to + 457 bp and *pARF19* fragment 2: - 4906 bp to -1992 bp. The amplified fragments were cloned either into pDONR P4P1R or into pENTR 5' TOPO plasmids by the Gateway BP-reaction or using the pENTR 5'-TOPO kit respectively. The resulting plasmids were recombined with the Gateway LR-reaction into both pMW2 and pMW3 Gateway destination vectors designed for yeast expression and containing respectively HIS3 or LacZ reporter genes (31). The resulting plasmids were transformed into YM4271 yeast strain.

Additional transcription factors were cloned and added to the existing root-specific transcription factor collection (Supplementary Table 10). The transcription factors were amplified by a PCR from the cDNA collections obtained by isolating total RNA from various tissues. The full-length transcription factor cDNA PCR product (without a stop codon) was inserted into a pENTR-Zeo plasmid by the Gateway BP reaction and then recombined into pDEST-AD-2μ destination vector designed for yeast expression and containing a GAL4 activation domain (31). The vectors were transformed into the yeast strain Yα1867.

To produce the reporter plasmid for the protoplast assays, the promoter fragment of the respective ARF corresponding to the one used in the eY1H assay and the ARF transcriptional reporter lines described above were amplified by PCR and cloned into pDONR P4-P1R plasmid. For the *ARF8* promoter a short part of the 35S promoter (-107 to +1) was inserted at position -115 bp. Separately, a construct containing NLS followed by mVenus coding sequence and an octopine synthase (OCS) terminator was cloned into pDONR 211 plasmid. Thirdly, a construct containing the promoter of RPS5a (promoter of the ribosomal protein S5A) driving TagBFP followed by a NLS signal and a nosT terminator were cloned into pDONR P2R-P3 plasmid. These three plasmids were recombined with a multisite Gateway to yield the final reporter plasmid pARF-NLS-mVenus-term-pRPS5a-TagBFP-NLS-term. An alternative reporter plasmid contained shorter ARF promoter fragment which contained sequences upstream and lacked sequences downstream of the start codon (corresponding to the transcriptional reporter lines with shorter promoters described above). For the effector plasmid for the protoplast assays, the RPS5 promoter was cloned into pDONR P4-P1R plasmid. The cDNA of the respective transcription factor without the stop codon was cloned into pDONR 211 plasmid. The construct contained the self-cleaving 2A peptide (32, 33) followed by mCherry coding sequence, a NLS and a nosT terminator and was cloned into the pDONR P2R-P3 plasmid. Finally, these three plasmids were recombined with a multisite Gateway reaction

to yield pRPS5a-cDNA-2A-mCherry-NLS-term. An alternative effector plasmid included an activator VP16 domain from the herpes simplex virus fused to the TF cDNA.

Microscopy

Roots of ARF transcriptional reporter lines were imaged at 5 days after germination. Plant cell walls were visualized by staining with 15 μg/ml propidium iodide solution. Roots were examined using a TCS-SP5 confocal microscope (Leica) with excitation at 514 nm and emission at 526-560 nm for mVenus and 605-745 nm for propidium iodide.

For analysis of shoot apical meristems, bolted shoots were dissected under a stereomicroscope and transferred to an Apex Culture Medium (1/2 MS medium supplemented with 1% sucrose, 0.8% agarose, 1x vitamin solution (myo-Inositol 100 mg/L, nicotinic acid 1 mg/L, pyridoxine hydrochloride 1 mg/L, thiamine hydrochloride 10 mg/L, glycine 2 mg/L)), for overnight incubation. Before microscopy cell walls were stained with 100 μg/ml propidium iodide solution. The shoot apices were then examined using a TCS-SP5 confocal microscope (Leica) with excitation at 514 nm and emission at 526-560 nm for mVenus and 605-745 nm for propidium iodide.

eY1H assay

The eY1H assay was conducted according to (31). The *ARF* promoters screened correspond in length and content to the ones used in the construction of the transcriptional reporter lines but the longer promoters were split into two fragments (*pARF5,8* and *19*; see Cloning). With the longer promoters, only 1 out of 39 TF was identified using the distal fragment of the *ARF8* promoter. This suggests that the other 38 TF bind in a region of the promoter going from -2480 bp to +134 bp for ARF5, -2120 bp to +42 bp for ARF8 and -1991 bp to + 457 bp for ARF19.

We used a TF collection enriched in root-expressed TFs (31) expanded with additional TFs involved either in development of the shoot apical meristem or in hormonal regulation (see Supplementary Table 10).

Transient expression analysis in *Arabidopsis thaliana* protoplasts

For the protoplast assay Col-0 seedlings were grown in short day conditions (8h light/16h dark) for 37-45 days. Leaves of similar size from the second or third pair were collected and digested in an enzyme solution (1% cellulose R10, 0.25% macerozyme R10, 0.4M mannitol, 10 mM CaCl2, 20 mM KCl, 0.1% BSA, 20 mM MES at pH 5.7) overnight at room temperature. Protoplasts were collected through a 70 micron mesh, washed twice with an ice-cold W5 solution (154 mM NaCl, 125 mM CaCl2, 5 mM KCl, 5 mM glucose, 2 mM MES at pH 5.7) and incubated on ice for 30 min. The protoplasts were then resuspended in MMG solution (0.4 M mannitol, 15 mM MgCl2, 4 mM MES at pH 5.7) with a final concentration 150 000 cells/ml. 10 µl of each the effector and the reporter plasmid DNA (concentration 3 mg/µl) were mixed with 200 µl of the protoplasts. Immediately, 220 µl of the PEG solution (40 % PEG 4000, 0.2 M mannitol, 0.1 M CaCl2) was added, incubated for 5 min at RT and then washed twice in W5 solution. The protoplasts were resuspended in 800 µl of the W5 solution and incubated for 24 hours in 16h light/8h dark growth chamber. Before imaging, the protoplasts were resuspended in 400 µl W5 solution and subsequently transformed into an 8-well imaging chamber.

A Zeiss 710 LSM confocal microscope was used for imaging the protoplasts (Extended Data Fig. 4). A sequential scanning was performed with mVenus (excitation at 514, emission at 520-559), TagBFP (excitation at 405 and emission at 423-491), mCherry (excitation at 561, emission at 598-636) and bright-field channels. Z-stacks of several protoplasts were taken. The data was analysed using ImageJ software. The image with the best focus for each protoplast was selected from the z-stack. The nucleus was selected and the mean fluorescence was measured as illustrated in Extended Data Fig. 4. The number of replicates was between 15-54

protoplasts with a majority of experiments including at least 20 protoplasts. For most ARF-TF interactions, 4 or 5 independent experiments were performed (Supplementary Table 4): 2-3 experiments with the standard effector plasmid and 2 experiments with alternative effector plasmid containing VP16 domain. For the statistical analysis, we first run a Kruskal-Wallis H-test on all controls for a given set of experiments (TF or TF-VP16). At a significance level of 0.05, all tests rejected the null hypothesis that control populations have the same median, indicating that the data could not be pooled. The results for each experiment was analyzed independently using a one-sided Mann-Whitney U-test to test for a significant effect of TF or TF-VP16 and to identify the direction of the change. To take into accounts the results from several experiments of a given type (TF or TF-VP16), we performed a meta-analysis using the Mudholkar & George's method (34) to combine the P-values from the independent experiments. This allows us to obtain a "meta P-values" per type of experiment. Note that the meta P-value was calculated only if the Mann-Whitney test was significant (with a significance level of 0.05) in at least one of the repetitions.

Expression analysis with qRT-PCR

The whole root and the whole shoot parts of the seedlings were collected separately. For one root sample, roots from 30 seedlings grown on the same plate were pooled together. For one shoot sample, 8 shoots from seedlings grown on the same plate were pooled together. Three independent replicates per genotype were collected. RNA was extracted using Spectrum Plant Total RNA kit (Sigma-Aldrich). The DNA was removed using TURBO DNA-free kit (Invitrogen). The cDNA was produced using SuperScript VILO cDNA Synthesis kit (Thermo Fischer) with 500 ng RNA. The cDNA was diluted 1:100 before use. The qRT-PCR was performed using Applied Biosystems Fast SYBR Green Master Mix. Expression of TUB4 gene was used as standard. The statistical analysis was performed with one-sided Mann-Whitney test

with $p < 0.1$ considered as statistically significant. *IAA 13* and *19* were chosen as auxin-responsive genes for qRT-PCR analysis in roots from (35).

Expression analysis of crosses between ARF transcriptional reporter lines and TF mutants

Mutants of the regulatory transcription factors were crossed with pARF7-mVenus transcriptional reporter line described above. The crosses were selected for the presence of homozygous pARF7-mVenus reporter construct. The F3 generation wild-type and mutant plants were compared.

The roots of 5 days old plants were stained with 15µg/ml propidium iodide and imaged using TCS-SP8 (Leica) confocal microscope with excitation at 514 nm and emission at 526-560 nm for mVenus and 605-745 nm for propidium iodide.

For the shoot microscopy the images were taken at Zeiss 710 LSM confocal microscope. mVenus intensity was measured separately in L1 and in L2/L3 layers in each of the 8 cross-sections with 50 nm distance between each cross-sections. Number of replicates: 7 wt and 7 mutant plants for *nf-yb13*, 12 wt and 12 mutant plants for *wrky38*.

Co-expression analysis of ARF transcriptional reporter lines and TF transcriptional reporter lines

Multisite Gateway cloning technology was used to generate TF transcriptional reporter lines. The promoter fragments of TFs were amplified by PCR with sequences: *pWRKY11* -3626 bp to -1 bp, *pDOF1.8* -4389 bp to -1 bp, *pAt2g26940* -3179 bp to -1 bp, *pAt2g44730* -2738 bp to -1 bp, *pCRF10* -4060 bp to -1 bp, *pZFP6* -2117 bp to -1 bp. The fragments were inserted into pDONR P4-P1R and recombined with 2x mCherry pDONR211 (containing double mCherry coding sequences) and N7 pDONR P2R-P3 (contaning nuclear localization signal) and pB7m34GW (the destination vector containing basta resistance gene for *in planta* selection) to

produce pTF-2xmCherryN7 constructs. These constructs were transformed in the *pARF*-mVenus transcriptional reporter lines backgrounds by floral dip method (30).

Roots of the plants grown for 5-10 days were imaged using the TCS-SP8 (Leica) confocal microscope, with excitation at 514 nm and emission at 526-560 nm for mVenus and excitation and emission at 587 nm and 610-670 nm respectively for mCherry. Total fluorescence was calculated for individual nuclei from two or three individual roots using a 6 px circular selection in imageJ (imageJ.net/Fiji). These values were then normalised for each channel based on a scale between 0-1 with one brightest nuclei in each root being set to a value of one. The shoots were examined using the TCS-SP8 (Leica) confocal microscope, with excitation at 514 nm and emission at 526-560 nm for mVenus and excitation and emission at 587 nm and 610-670 nm respectively for mCherry.

Inducible overexpression of TFs

Multisite Gateway cloning technology was used to generate TF inducible overexpression lines. The chimeric transcription activator p1R4-pG1090:XVE (36) containing XVE followed by the *rbs* and *nos* terminators and LexA operon, expressed under UBQ10 promoter was recombined with TF coding sequence (lacking STOP codon) in pDONR211 and the 2A-mCherry-term pDONR P2R-P3 (containing the self-cleaving 2A peptide (32, 33) followed by mCherry coding sequence, a NLS and a nosT terminator) and pB7m34GW (the destination vector containing basta resistance gene for *in planta* selection) to produce pUBQ10-XVE-TF-2A-mCherry estradiol-inducible constructs. These constructs were transformed in the pARF7-mVenus transcriptional reporter line background by floral dip method (30).

For the overexpression analysis, roots of the plants grown for 5 days were treated with 10μM β-estradiol for 24h and imaged using the TCS-SP8 (Leica) confocal microscope, with excitation at 514 nm and emission at 526-560 nm for mVenus and excitation and emission at 587 nm and 610-670 nm respectively for mCherry.

Shoot phenotype analysis of the TF mutants

24 T-DNA insertion mutants and the wild-type Col-0 were grown in 8h light/16h dark conditions on soil for 43 days. Leaf number was counted every 3 days starting from day 24. Rosette diameter was measured at 43 days. After 43 days of growth in the above conditions, the plants were transferred to 16h light/8h dark conditions to induce bolting. The following parameters were measured at 21 and 27 days in the 16h light/8h dark conditions: length of the main stem, number of cauline branches growing from the main stem, number of axillary branches growing from rosette (the main stem not included). The number of replicates per genotype was 12 plants. For the statistical analysis an unpaired two-tailed t-test was conducted with $p \leq 0.05$ considered as statistically significant.

Root phenotype analysis of the TF mutants

For root length measurement and for gravitropic analysis plants were grown on ½ MS medium supplemented with 1% agar in 12h light/12h dark conditions. For root length analysis, plants were grown either on medium lacking IAA or supplemented with 10 μM IAA. To reduce plate-to-plate variation wild-type plants and mutants were grown on the same agar plate. Images were taken at 15 days and the root length was measured. The number of replicates per genotype was at least 26 plants without IAA and 15 plants with IAA. For the gravitropic response, plants were grown for 5 days, then turned at a 90° angle and images taken every 1 hour for 12h hours in the dark using an infrared camera. The number of replicates per genotype was at least 26 plants. Rootnav v1.8 software (https://www.nottingham.ac.uk/research/groups/cvl/software/rootnav.aspx) was used for data analysis. Statistical analysis was done with unpaired two-tailed t-test with $p \leq 0.05$ considered as statistically significant.

***In situ* hybridization**

For RNA probe synthesis, 300-500 bp templates were amplified from a cDNA library adding the T7 RNA polymerase promoter sequence at the 5' prime overhang. The product was gel purified and used directly as a template for transcription with DIG RNA Labeling Kit (SP6/T7, Roche). The following primers were used: 3'-ctggttgcagctctggtagagt-5' and 3'-ggatcctaatacgactcactatagggaggcagcggtgagtttgtggaatcc-5' (ARF5); 3'-gctgctgttgtttccgctatgt-5' and 3'-ggatcctaatacgactcactatagggaggggtttgacattccgttcggcat-5' (ARF6); 3'-tgcctgatggaaggggtgattt-5' and 3'-ggatcctaatacgactcactatagggaggtgctgcggaagattctcactca-5' (ARF8). Roots were cut from 4 days old plants and vacuum-infiltrated in FAA (50% (v/v) ethanol, 5% (v/v) acetic acid, 3.7% (v/v) formaldehyde) 3-4 times for 5 min each and then fixed overnight at 4 °C. The tissue was rinsed with PBS 4 time for 15 min and embedded in in 1% SeaKem LE-agarose (in PBS). For paraffin-embedding, a Leica ASP200 vacuum tissue processor was used following the program described in Smetana et al. 2019 (37). The samples were cut into 7 µm sections. During pre-treatment the samples were passed through the following solution series: xylene 2 times 10 min, methanol 5 min, 100% (v/v) ethanol 2 times 2 min, 95% ethanol 1 min, 90% ethanol 1 min, 80% ethanol 1 min, 60% ethanol + 0.75% NaCl 1 min, 30% ethanol + 0.75% NaCl 1 min, 0.75% NaCl 2 min, PBS 2 min, 1µg/ml Proteinase K in dilution buffer (100 mM Tris pH 7.5, 50 mM EDTA, pH 7.5) 30 min at 37°C, PBS + Glycine (2 mg/ml) 2 min, PBS 2 min, FAA 5 min, 2 times PBS 5 min, 0.75% NaCl 2 min, 30% ethanol + 0.75% NaCl 30 sec, 60% ethanol + 0.75% NaCl 30 sec, 80% ethanol 30 sec, 90% ethanol 30 sec, 95% ethanol 30 sec, 2 times 100% ethanol 30 sec. The probe (0.3 ug/ml/kb probe complexity) was mixed with hybridization solution (50% formamide, 10 % dextran sulphate, Denhardt's solution, 500 µg/ml tRNA, 5 mM EDTA, 300 mM NaCl, 10 mM Tris pH 7.0, 10 mM Sodium phosphate pH 7.0), denatured at 80°C for 2 min and applied to the samples which were placed into the wet chamber aligned with paper towels soaked in the soaking solution (2xSSC in 50% formamide). The samples were hybridized overnight at 50°C. The

samples were washed with 0.2xSSC 4 times for 30 min, 0.2xSSC 37°C 5 minutes, 0.2xSSC RT 5 min, PBS 5 min. Detection was done by incubating the samples in 1 % blocking solution (1% Blocking reagent,100 mM Tris-HCl pH7.5, 150 mM NaCl, 0.3% TritonX-100) for 45 min, then in a wet chamber with antibody solution (anti-Digoxigenin-AP 1:1250 in 1 % blocking solution) for 1.5h, washed with BufferA (1% BSA in 100 mM Tris-HCl pH7.5, 150 mM NaCl, 0.3% TritonX-100) 3 times for 30 minutes, washed with the detection buffer (100 mM Tris pH 9.5, 100 mM NaCl, 50 mM MgCl2) 2 times 5 min, applied 200 µl of color substrate solution (4.5 ml detection buffer + 90 µl NBT-BCIP) and incubate 24h for ARF5 and ARF6, and o/n ARF8 at RT. The reaction was stopped by washing the samples with TE-buffer 2 times 5 min. The samples were mounted in 50% glycerol and observed under the light microscope.

In silico analyses

Analysis of expression and function of regulatory TFs

Expression of TFs in the root and the shoot apical meristems was analysed using cell type-specific expression profiles from (38, 39, 440).

Overrepresentation of TF gene families was analysed for families represented by two or more members in the network. The number of gene family members in the network was compared to total number of genes from this family in the TF library. Statistical analysis was done using a hypergeometric test with $p \leq 0.05$ considered as statistically significant.

Involvement of TFs in specific developmental processes (development, biotic and abiotic stress) was analysed based on literature description.

Chromatin state analysis

Binary data on H3K27me3- and H3K4me3 marked genes and chromatin accessibility regions were retrieved from multiple datasets covering a range of tissues and developmental stages. For each dataset, at least two biological replicates were considered and only the presence of a given

ARF in both gene lists was scored as a positive association with a chromatin mark or an accessible region.

Datasets used for chromatin marking analysis were: H3K27me3 from (17, 41, 42, 43, 44, 45) (GEO database GSE24657, GSE7907, GSE24507, GSE50636, GSE24657, GSE24710, GSE19654; ArrayExpress database E-MTAB-4680, E-MTAB-4684) and H3K4me3 from (17, 41, 42, 43, 44) (GEO GSE24658, GSE7907, GSE50636, GSE24665, GSE19654; ArrayExpress E-MTAB-4680, E-MTAB-4684).

Datasets used for chromatin accessibility analysis were: DNase I hypersensitive sites from (46) (GEO GSM1289358, GSM1289362, GSM1289374), FANS-ATAC-defined accessible regions from (47) (GEO GSM2260231, GSM2260232, GSM2260235, GSM2260236) and ATAC-defined transposase hypersensitive sites from (48, 49) (GEO GSM2704255, GSM2704256, GSM2719200, GSM2719202, GSM2719203, GSM2719203, GSM2719204, GSM2719205). For each chromatin accessibility dataset, the presence of at least one accessible region within the *ARF* gene and up to 1 kb upstream of its transcription start site was scored using *ad hoc* scripts.

Visualization of epigenomic data was carried out using the IGV software (50, 51).

Binding motif search and reanalysis of DAP-Seq data

Position weight matrices (PWM) available for TFs identified in the eY1H screen were retrieved from Jaspar (52) and CisBP (53) databases. Using these PWMs, we computed the best score of the TF binding sites present in each Arabidopsis 2kb promoter with an R script using the Biostrings library (https://bioconductor.org/packages/release/bioc/html/Biostrings.html) and ranked the ARF^{ClassA} promoter among all Arabidopsis promoters based on this score. As negative control, this operation was repeated identically 5 times for each ARF^{classA} promoter with 20 randomly-selected TFs (excluding specific TF classes/families identified in the eY1H screen). The distribution of ARF^{ClassA} promoter ranks with eYI1H-selected and randomly-selected TFs were compared using a one-sided t-test.

DAP-seq files containing the peak list from (20) were retrieved (GEO accession number GSE60141). Bedtools intersect (bedtools.readthedocs.io/en/latest/index.html) was then used with the –wb option to determine which DAP peak overlap with each promoter.

Methods References

30. Clough, S. J. & Bent, A. F. Floral dip: a simplified method for Agrobacterium-mediated transformation of Arabidopsis thaliana. *Plant J.* **16**, 735–743 (1998).

31. Gaudinier, A. *et al.* Enhanced Y1H assays for Arabidopsis. *Nat Methods* **8,** (2011).

32. Kim, J. H. *et al.* High cleavage efficiency of a 2A peptide derived from porcine teschovirus-1 in human cell lines, zebrafish and mice. *PLoS ONE* **6**, e18556 (2011).

33. Trichas, G., Begbie, J. & Srinivas, S. Use of the viral 2A peptide for bicistronic expression in transgenic mice. *BMC Biol.* **6**, 40 (2008).

34. George, E. O. & Mudholkar, G. S. On the convolution of logistic random variables. *Metrika* **30**, 1–13 (1983).

35. Paponov, I. A. *et al.* Comprehensive transcriptome analysis of auxin responses in Arabidopsis. *Mol Plant* **1**, 321–337 (2008).

36. Siligato R et al., MultiSite Gateway-Compatible Cell Type-Specific Gene-Inducible System for Plants. *Plant Physiol.* **170**, 627–641 (2016).

37. Smetana, O. *et al.* High levels of auxin signalling define the stem-cell organizer of the vascular cambium. *Nature* **565**, 485–489 (2019).

38. Brady, S. M. *et al.* A high-resolution root spatiotemporal map reveals dominant expression patterns. *Science* **318**, 801–806 (2007).

39. Yadav, R. K., Girke, T., Pasala, S., Xie, M. & Reddy, G. V. Gene expression map of the Arabidopsis shoot apical meristem stem cell niche. *Proc. Natl. Acad. Sci. U.S.A.* **106**, 4941–4946 (2009).

40. Yadav, R. K., Tavakkoli, M., Xie, M., Girke, T. & Reddy, G. V. A high-resolution gene expression map of the Arabidopsis shoot meristem stem cell niche. *Development* **141**, 2735–2744 (2014).

41. Oh, S., Park, S. & van Nocker, S. Genic and global functions for Paf1C in chromatin modification and gene expression in Arabidopsis. *PLoS Genet.* **4**, e1000077 (2008).

42. Willing, E.-M. *et al.* Genome expansion of Arabis alpina linked with retrotransposition and reduced symmetric DNA methylation. *Nat Plants* **1**, 14023 (2015).

43. Deal, R. B. & Henikoff, S. A simple method for gene expression and chromatin profiling of individual cell types within a tissue. *Dev. Cell* **18**, 1030–1040 (2010).

44. You, Y. *et al.* Temporal dynamics of gene expression and histone marks at the Arabidopsis shoot meristem during flowering. *Nat Commun* **8**, 15120 (2017).

45. Lafos, M. *et al.* Dynamic regulation of H3K27 trimethylation during Arabidopsis differentiation. *PLoS Genet.* **7**, e1002040 (2011).

46. Sullivan, A. M. *et al.* Mapping and dynamics of regulatory DNA and transcription factor networks in A. thaliana. *Cell Rep* **8**, 2015–2030 (2014).

47. Lu, Z., Hofmeister, B. T., Vollmers, C., DuBois, R. M. & Schmitz, R. J. Combining ATAC-seq with nuclei sorting for discovery of cis-regulatory regions in plant genomes. *Nucleic Acids Res.* **45**, e41 (2017).

48. Maher, K. A. *et al.* Profiling of Accessible Chromatin Regions across Multiple Plant Species and Cell Types Reveals Common Gene Regulatory Principles and New Control Modules. *Plant Cell* **30**, 15–36 (2018).

49. Sijacic, P., Bajic, M., McKinney, E. C., Meagher, R. B. & Deal, R. B. Changes in chromatin accessibility between Arabidopsis stem cells and mesophyll cells illuminate cell type-specific transcription factor networks. *Plant J.* **94**, 215–231 (2018).

50. Thorvaldsdóttir, H., Robinson, J. T. & Mesirov, J. P. Integrative Genomics Viewer (IGV): high-performance genomics data visualization and exploration. *Brief. Bioinformatics* **14**, 178–192 (2013).

51. Robinson, J. T. *et al.* Integrative Genomics Viewer. *Nat Biotechnol* **29**, 24–26 (2011).

52. Khan, A. *et al.* JASPAR 2018: update of the open-access database of transcription factor binding profiles and its web framework. *Nucleic Acids Res.* **46**, D260–D266 (2018).

53. Weirauch, M. T. *et al.* Determination and inference of eukaryotic transcription factor sequence specificity. *Cell* **158**, 1431–1443 (2014).

54. Berger, N., Dubreucq, B., Roudier, F., Dubos, C. & Lepiniec, L. Transcriptional regulation of Arabidopsis LEAFY COTYLEDON2 involves RLE, a cis-element that regulates trimethylation of histone H3 at lysine-27. *Plant Cell* **23,** 4065–4078 (2011).

55. Yu, C.-P., Lin, J.-J. & Li, W.-H. Positional distribution of transcription factor binding sites in Arabidopsis thaliana. *Sci Rep* **6,** 25164 (2016).

56. Goda, H. *et al.* The AtGenExpress hormone and chemical treatment data set: experimental design, data evaluation, model data analysis and data access. *Plant J.* **55**, 526–542 (2008).

Acknowledgements

We thank Fabrice Besnard, Antoine Larrieu and Romain Azaïs for their help with data analysis and statistics; Mikko Herpola for the RNA in situ hybridization analysis; Giuseppe Castiglione for help with root phenotyping; Anthony Mathelier for help with JASPAR; Dolf Weijers for ARF transcriptional reporter lines. This work was supported by a joint INRA/University of Nottingham PhD grant to J.T.; ANR-2014-CE11-0018 grant (Serrations) and Human Frontier Science Program organization (HFSP) grant RPG0054-2013 to T.V.; a Royal Society University Research Fellowship and enhancement award (UF110249 and RGF\EA\180308) to

A.B.; a starting grant from the Programme Avenir Lyon Saint Etienne (ANR-11-IDEX-0007) to F.R; an HHMI Faculty Scholar fellowship to S.M.B.; ANR-10-LABX-49-01 and ANR-17-EURE-0003 to F.P.; ANR-18-CE12-0014-02 to T.V., F.R. and F.P.; Aux-ID CNRS PICS grant to T.V., A.B. and E.F..

Author Contribution

A.B. and T.V. designed the study and supervised the work; J.T. and F.P., F.R., E.F., S.M.B., A.B. and T.V. designed the experiments; J.T., A-M. B. and M.E.S performed the eY1H screen with the help of S.P. and M.B.; J.T, J.H., E.C., C. G.-A., S.L., G.B. performed all experiments in relation with TF biological activity characterization; J.L. performed the statistical analysis of the protoplast experiment and participated in all statistical analysis; O.S. and A.-P..M performed the *in situ* hybridization experiments; A.S. and F.P. performed the TF binding site analysis; S.B. and E.F. performed the modeling analysis; J.M. and F.R. performed the epigenetic data analysis; all authors were involved in data analysis; J.T., A.B. and T.V. wrote the manuscript with inputs from all authors.

Financial competing interests

The authors declare no competing interests.

Additional Information

Supplementary information is available for this paper. Correspondence and request for materials should be addressed to T.V. (teva.vernoux@ens-lyon.fr) or A.B. (Anthony.Bishopp@nottingham.ac.uk).

Data availability

The data including the source data that supports the finding of this study are available within the paper, its supplementary information files or publicly-available datasets. Publicly-available position weight matrices were obtained from Jaspar and CisBP databases. Publicly-available chromatin marking and accessibility datasets were acquired from the GEO and ArrayExpress databases with the following accession numbers: GSE24665, GSE24658, GSE7907,

GSE24507, GSE50636, GSE24657, GSE24710, GSE19654, GSM2260231, GSM2260232, GSM2260235, GSM2260236, GSM2704255, GSM2704256, GSM2719200, GSM2719202, GSM2719203, GSM2719204, GSM2719205, GSM1289362, GSM1289374, E-MTAB-4680, E-MTAB-4684, GSM1289358.

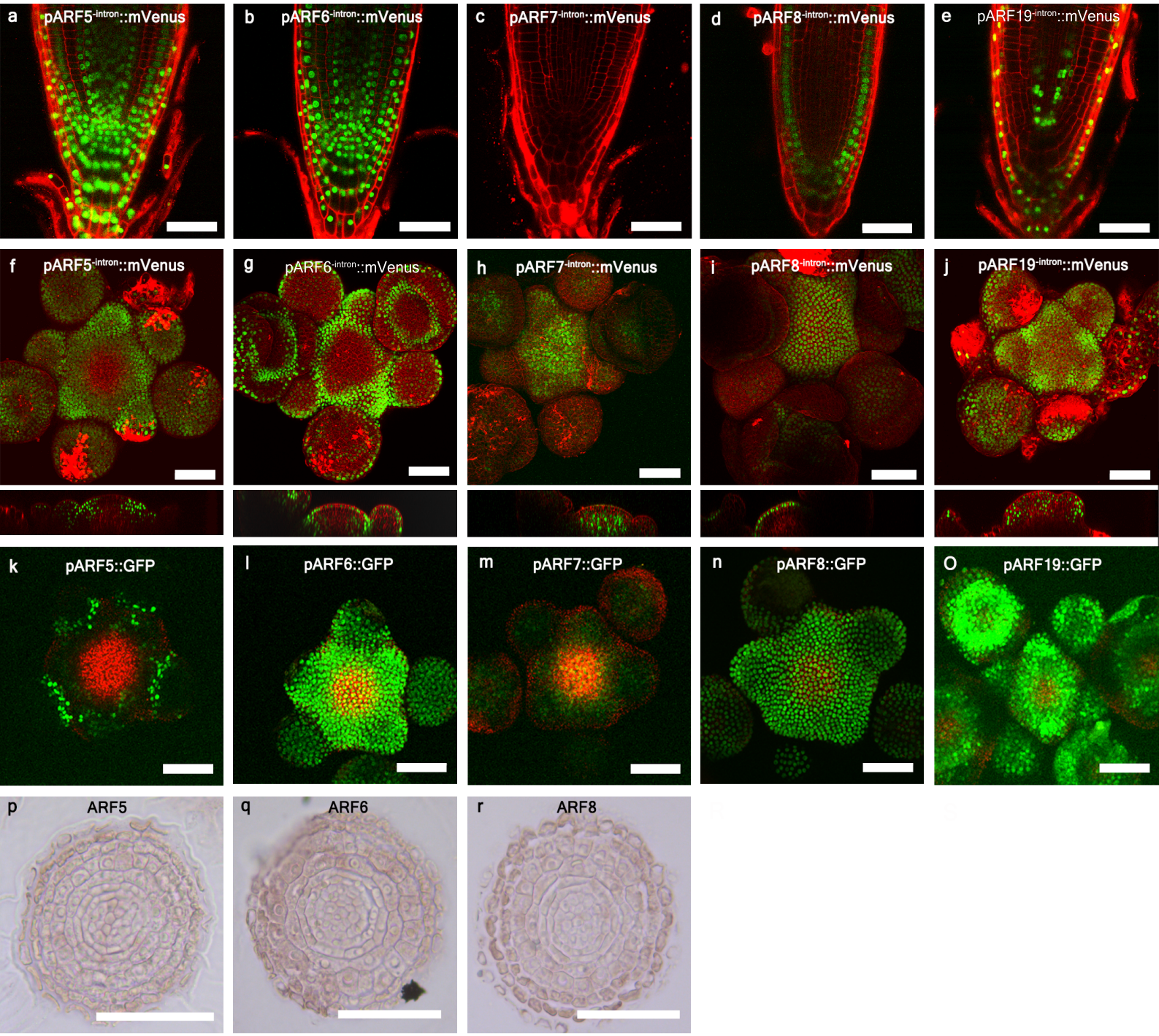
a pARF5-intron::mVenus
b pARF6-intron::mVenus
c pARF7-intron::mVenus
d pARF8-intron::mVenus
e pARF19-intron::mVenus
f pARF5-intron::mVenus
g pARF6-intron::mVenus
h pARF7-intron::mVenus
i pARF8-intron::mVenus
j pARF19-intron::mVenus
k pARF5::GFP
l pARF6::GFP
m pARF7::GFP
n pARF8::GFP
O pARF19::GFP
p ARF5
q ARF6
r ARF8

Extended data figure legends

Extended Data Fig.1 Analysis of *ARF*^{ClassA} expression in the RAM and the SAM using transcriptional reporter lines and *in situ* hybridisation

(a-j) Confocal images showing expression of *ARF5* (a,f), *ARF6* (b,g), *ARF7* (c,h), *ARF8* (d,i) and *ARF19* (e,j) in the RAM and the SAM using promoters that lack sequences downstream of the start codon but contain the long upstream sequences (*pARF* $^{-\ intron}$*::mVenus*) (ca. 3 kb for *ARF6* and *ARF7*; 5 kb for *ARF5*, *ARF8* and *ARF19*) (see Methods). For SAM images (f-j) an orthogonal projection is shown below to provide information about expression in different layers. For comparison, panels k-o show expression of each *ARF*^{ClassA} in the SAM using the previously published *pARF::GFP* lines with shorter ca. 2 kb promoters containing sequences upstream of the start codon (14). *ARF5* (k), *ARF6* (l), *ARF7* (m), *ARF8* (n) and *ARF19* (o). (p-r) *In situ* hybridisations through the RAM for *ARF5* (p), *ARF6* (q) and *ARF8* (r). Note that expression patterns of the *ARF*^{ClassA} reporters (a-j) differed from those with shorter 2 kb promoters (k-o, (14)), and recapitulate the patterns observed with RNA *in situ* hybridization (p-r; (16)). This was particularly clear in the shoot for *ARF5* and *6*. Shorter promoters drive GFP expression mostly in flower boundaries for *ARF5* and throughout the meristem for *ARF6*, in contrast with detection of both genes throughout the periphery of the meristem both with longer promoters (k-o; also Fig.1f-j) or using *in situ* hybridization (15). Experiments were done three times (a-e) and two times (f-r). Scale bars: 50 µm.

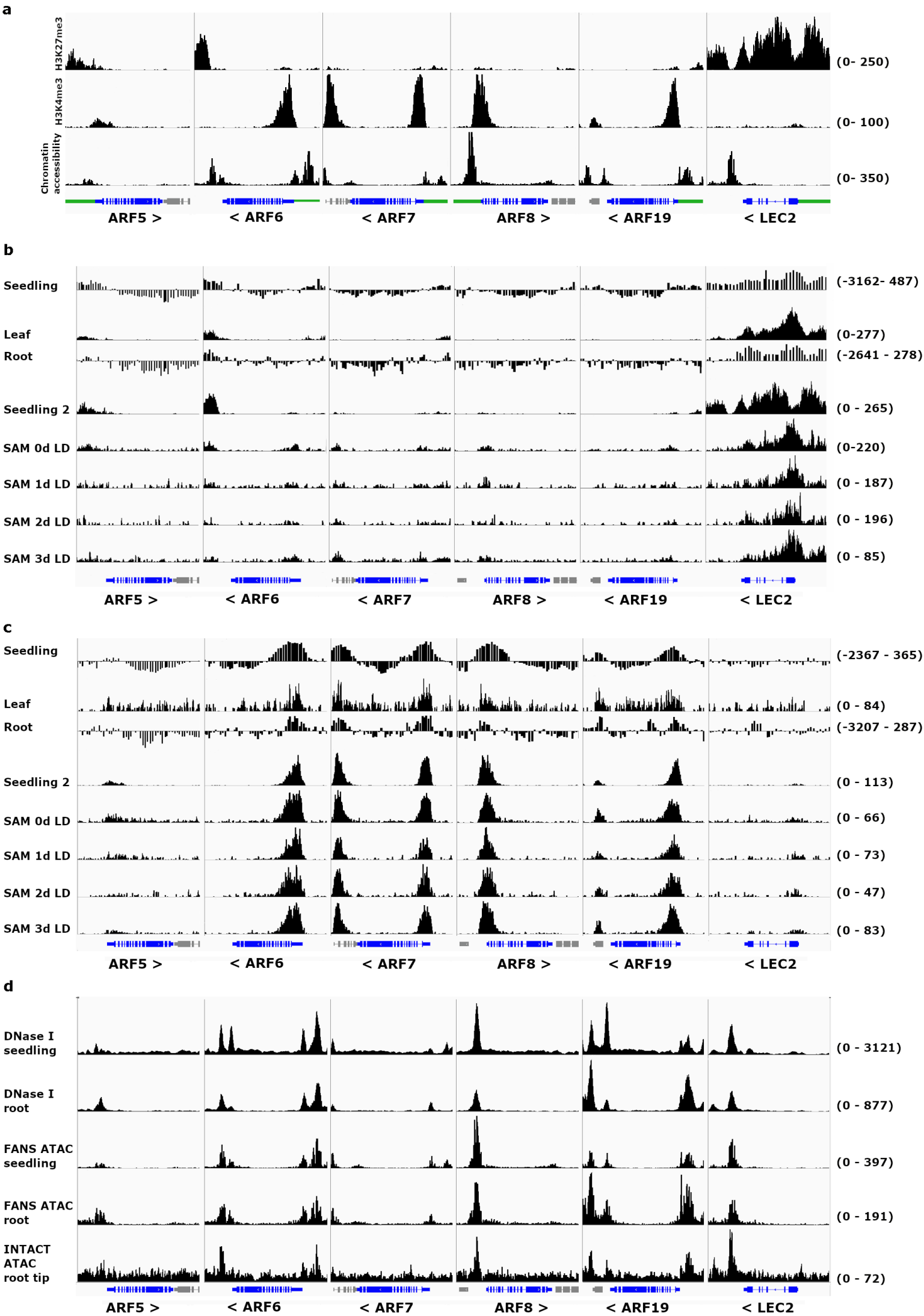
a
H3K27me3
H3K4me3
Chromatin accessibility
(0- 250)
(0- 100)
(0- 350)
ARF5 >
< ARF6
< ARF7
ARF8 >
< ARF19
< LEC2
b
Seedling
Leaf
Root
Seedling 2
SAM 0d LD
SAM 1d LD
SAM 2d LD
SAM 3d LD
(-3162- 487)
(0-277)
(-2641 - 278)
(0 - 265)
(0-220)
(0 - 187)
(0 - 196)
(0 - 85)
ARF5 >
< ARF6
< ARF7
ARF8 >
< ARF19
< LEC2
c
Seedling
Leaf
Root
Seedling 2
SAM 0d LD
SAM 1d LD
SAM 2d LD
SAM 3d LD
(-2367 - 365)
(0 - 84)
(-3207 - 287)
(0 - 113)
(0 - 66)
(0 - 73)
(0 - 47)
(0 - 83)
ARF5 >
< ARF6
< ARF7
ARF8 >
< ARF19
< LEC2
d
DNase I seedling
DNase I root
FANS ATAC seedling
FANS ATAC root
INTACT ATAC root tip
(0 - 3121)
(0 - 877)
(0 - 397)
(0 - 191)
(0 - 72)
ARF5 >
< ARF6
< ARF7
ARF8 >
< ARF19
< LEC2

Extended Data Fig.2 Distribution of the repressive chromatin marker H3K27me3, the active chromatin marker H3K4me3 and chromatin accessibility at *ARF*$^{class\ A}$ loci.

(a) Chromatin landscape of *ARF*^{ClassA} and *LEC2* in whole seedlings illustrating the chromatin status of *ARF*^{ClassA} loci. Repressive H3K27me3 marker (top row), active H3K4me3 marker (middle row) and FANS-ATAC chromatin accessibility (bottom row; see Supplementary Table 1). (b,c) Chromatin landscape of *ARF*^{ClassA} and *LEC2* loci showing distribution of the repressive chromatin marker H3K27me3 (a) the active chromatin marker H3K4me3 (b) in various tissues. Seedling = whole seedlings (17), Leaf = rosette leaves (42), Root = whole roots (17), Seedling 2 = whole seedlings (44), SAM = shoot apical meristems after 0, 1, 2 or 3 days in long-day conditions (44). Gene models are shown below with arrowheads indicating direction of transcription. (d) The chromatin landscape of *ARF*^{ClassA} and *LEC2* loci showing chromatin accessibility in various tissues. DNaseI-seq seedling: DNase I hypersensitive sites in whole seedling (46); DNaseI-seq root: DNase I hypersensitive sites in root (46); FANS-ATAC seedling: FANS-ATAC accessible regions in whole seedling (47); FANS-ATAC roots: FANS-ATAC accessible regions in roots (47); INTAC-ATAC root tip: INTACT-ATAC transposase hypersensitive sites in root tips (48). The *LEC2* locus is included as a negative control for H3K4me3 marking and chromatin accessibility, and as a positive control for H3K27me3 marking (54). The y axis scales are shown to the right and show the minimum and maximum number of reads represented in each windows of the same row, except for the dataset related to (17) for which the data range corresponds to the IP/INPUT value of the ChIP-chip experiments. For the x-axis the window size is fixed at 8.5 kb and centered on the gene of interest (gene model in blue below each column, 5' sequences in green), with arrowheads by the gene name showing the direction of the locus.

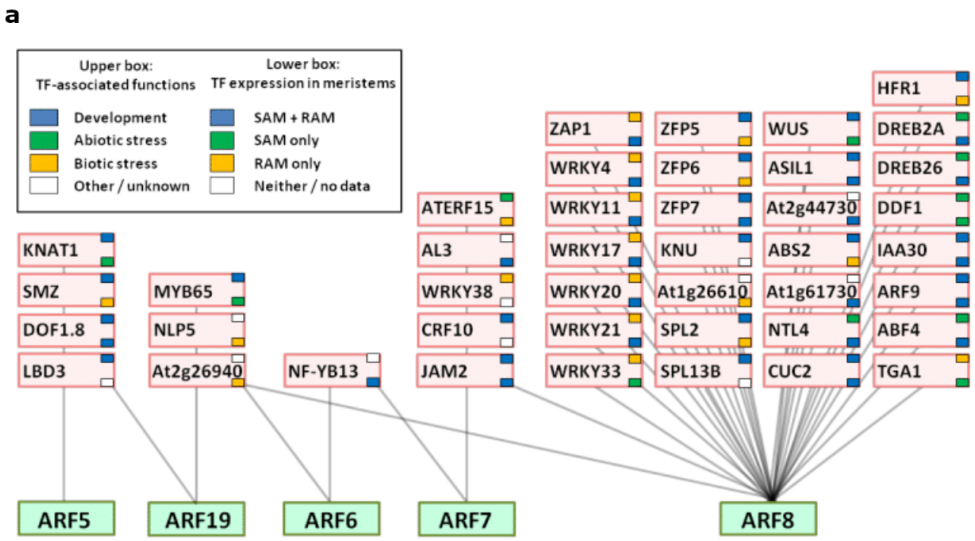
a
Upper box:
TF-associated functions
Lower box:
TF expression in meristems
Development
Abiotic stress
Biotic stress
Other / unknown
SAM + RAM
SAM only
RAM only
Neither / no data
KNAT1
SMZ
DOF1.8
LBD3
MYB65
NLP5
At2g26940
NF-YB13
ATERF15
AL3
WRKY38
CRF10
JAM2
ZAP1
WRKY4
WRKY11
WRKY17
WRKY20
WRKY21
WRKY33
ZFP5
ZFP6
ZFP7
KNU
At1g26610
SPL2
SPL13B
WUS
ASIL1
At2g44730
ABS2
At1g61730
NTL4
CUC2
HFR1
DREB2A
DREB26
DDF1
IAA30
ARF9
ABF4
TGA1
ARF5
ARF19
ARF6
ARF7
ARF8

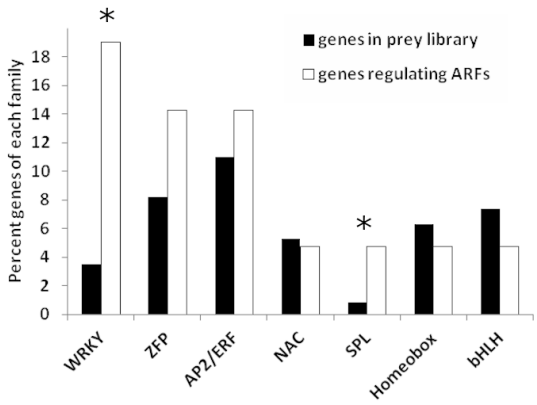
b
genes in prey library
genes regulating ARFs
Percent genes of each family
0
2
4
6
8
10
12
14
16
18
*
*
WRKY
ZFP
AP2/ERF
NAC
SPL
Homeobox
bHLH

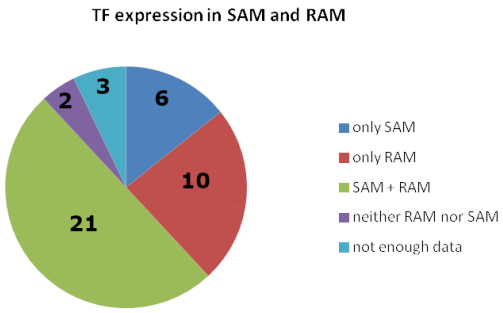
c
TF expression in SAM and RAM
6
10
21
2
3
only SAM
only RAM
SAM + RAM
neither RAM nor SAM
not enough data

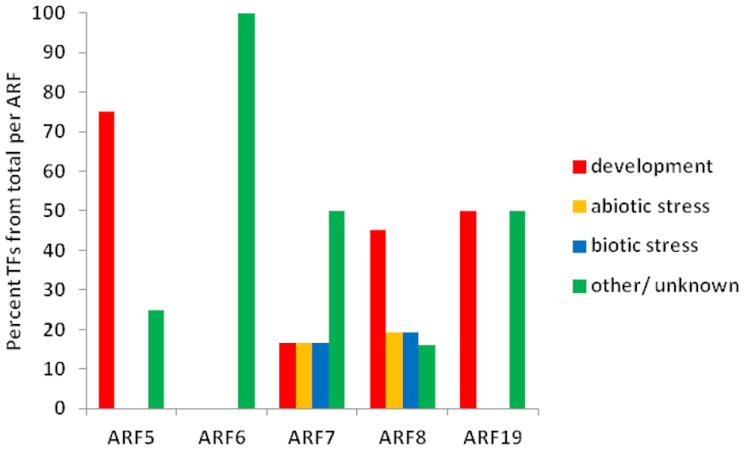
d
Percent TFs from total per ARF
0
10
20
30
40
50
60
70
80
90
100
ARF5
ARF6
ARF7
ARF8
ARF19
development
abiotic stress
biotic stress
other/ unknown

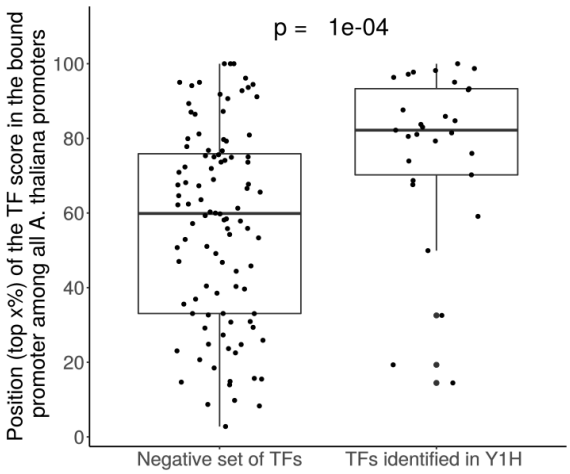
e
p = 1e-04
Position (top x%) of the TF score in the bound promoter among all A. thaliana promoters
0
20
40
60
80
100
Negative set of TFs
TFs identified in Y1H

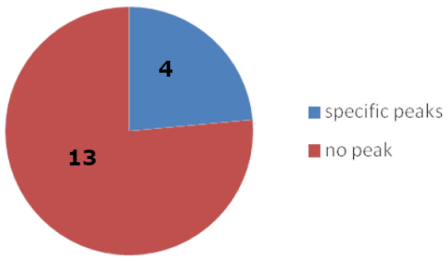
f
TF binding in DAP-seq
4
13
specific peaks
no peak

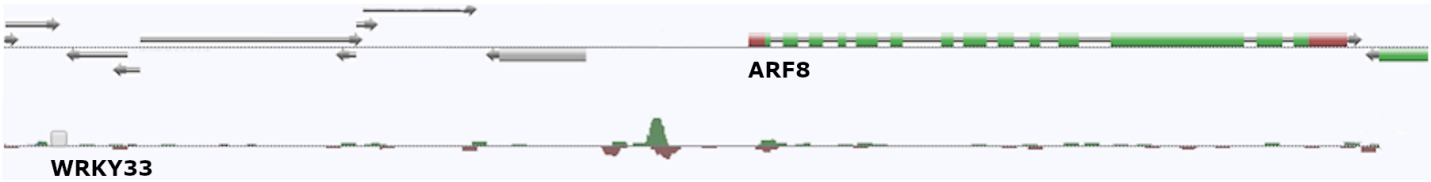
g
ARF8
WRKY33

Extended Data Fig.3 Characterisation of the TFs and TF binding sites that regulate *ARF*$^{Class\ A}$ expression.

(a) Yeast one-hybrid promoter-transcription factor interaction network for *ARF*^{ClassA}. Green boxes correspond to the *ARF*^{ClassA}; pink boxes are transcription factors binding to the *ARF* promoters. TF-associated functions and expression analysis are indicated in the upper and lower small boxes and color-coded as indicated in the key. Note that when two promoter fragments were used for the screen (see Methods), 35 out of 36 regulators bound to the more proximal fragment, supporting previous observations that the majority of transcription factor binding sites reside within a few kb of the transcriptional start site (55). (b) Frequency of TF gene families in the Y1H library collection (black) and in the Y1H network (white). Only families represented by at least two members in the Y1H network were analyzed. The network is overrepresented with members of the WRKY and SPL TF families. Statistical analysis: hypergeometric test significant to 5% (*; p = 4e-05 for WRKY family and p = 0.044 for SPL family). Sample size for TFs in Y1H library in black/Y1H network in white: n = 29/8 TFs (WRKY) ; n = 68/6 (ZFP); n = 91/6 (AP2/ERF); n = 44/2 (NAC); n = 7/2 TFs (SPL); n = 52/2 TFs (Homeobox); n = 61/2 TFs (bHLH). (c) TF expression in the RAM (38) and the SAM (39, 40). 50% of the identified TFs are expressed in both shoots and roots while 24% and 14% are expressed specifically in roots or shoots respectively. (d) Known functions of the TFs in the Y1H network based on a literature search (see also Supplementary Table 2). (e) Boxplot representation of the distribution of *ARF*^{ClassA} promoter ranks. For TFs with established binding models, we ranked *ARF*^{ClassA} promoters among all Arabidopsis promoters based on the score of the predicted TF binding sites. We repeated the same operation with a set of randomly chosen TFs from different families (see Methods). The comparison of rank distributions with those of a set of randomly chosen TFs from different families revealed significantly higher ranks for eY1H-identified TFs (see also Supplementary Table 3). Statistical analysis: one-sided t-test. Sample size: n = 29 for eY1H-selected TFs and n = 100 for randomly-selected TFs . Data

are represented as boxplots where the middle line is the median, the lower and upper hinges correspond to the first and third quartiles, the upper whisker extends from the hinge to the largest value no further than 1.5 × IQR from the hinge (where IQR is the inter-quartile range) and the lower whisker extends from the hinge to the smallest value at most 1.5 × IQR of the hinge. All the individual values are plotted. (f) Summary of the DAP-seq analysis for the 17 TFs (see also Supplementary Table 3). (g) Example of DAP-Seq data, here a DAP-seq peak for WRKY33 in the promoter of *ARF8*. DAP-Seq (f,g) thus confirms experimentally inferred bindings (e) for 4 out of the 17 (24%) TFs for which DAP-Seq data are available (see also Supplementary Table 3). Note also that chromatin immunoprecipitation sequencing (ChIP-Seq) confirm binding of WUSCHEL to *ARF8* promoter (21).

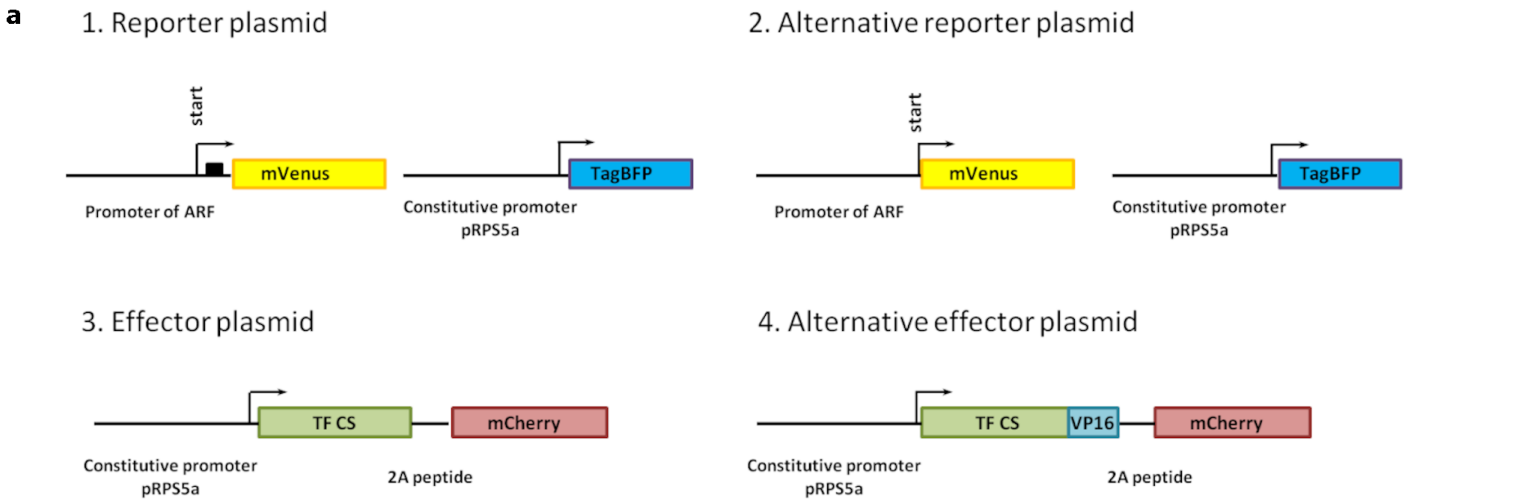
a
1. Reporter plasmid
start
mVenus
TagBFP
Promoter of ARF
Constitutive promoter
pRPS5a
2. Alternative reporter plasmid
start
mVenus
TagBFP
Promoter of ARF
Constitutive promoter
pRPS5a
3. Effector plasmid
TF CS
mCherry
Constitutive promoter
pRPS5a
2A peptide
4. Alternative effector plasmid
TF CS
VP16
mCherry
Constitutive promoter
pRPS5a
2A peptide

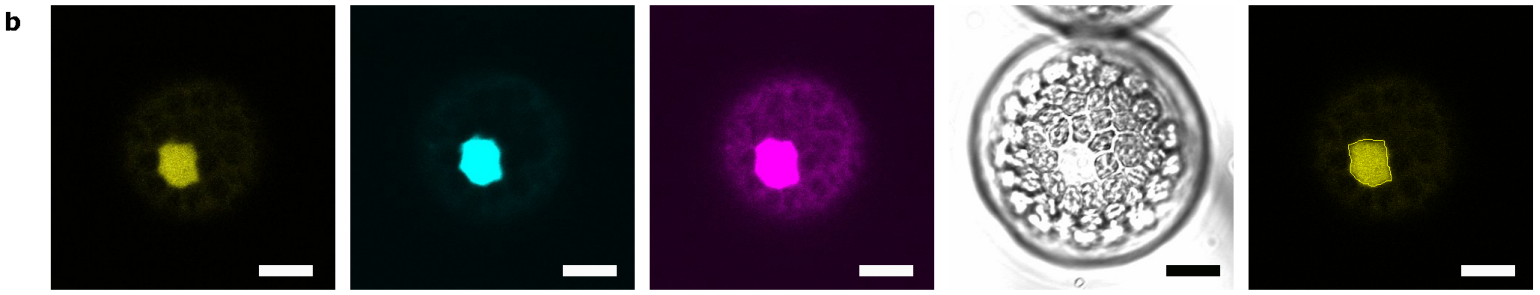
b
mVenus
Tag BFP
mCherry
Bright Field
Quantification

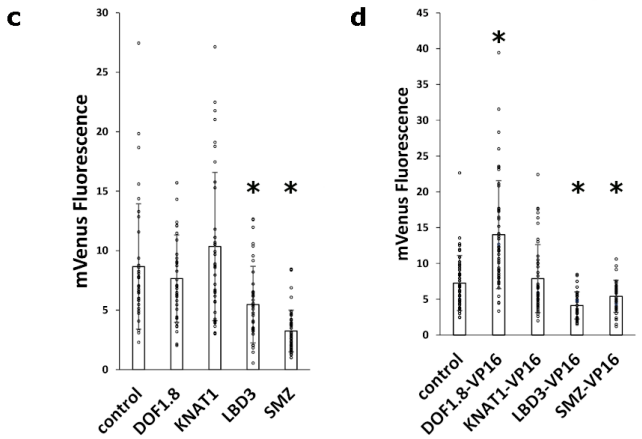
c
mVenus Fluorescence
30
25
20
15
10
5
0
*
*
control
DOF1.8
KNAT1
LBD3
SMZ

d
mVenus Fluorescence
45
40
35
30
25
20
15
10
5
0
*
*
*
control
DOF1.8-VP16
KNAT1-VP16
LBD3-VP16
SMZ-VP16

Extended Data Fig.4 Methodology used for the transient protoplast assay.

(a) Design of the standard reporter plasmid containing upstream and downstream sequences of the *ARF* promoter including the first intron (1.), the alternative reporter plasmid containing only upstream sequences of the ARF promoter (2.), the standard effector plasmid (3.), and an alternative effector plasmid containing the VP16 domain fused to the TF coding sequence (4.). (b) Example of a nucleus of a transformed living protoplast imaged with confocal microscopy with channels for mVenus, TagBFP, mCherry and bright-field. The presence of TagBFP specifically in the nucleus is used as a transformation control and as a test of viability of the protoplasts. Quantification: definition of the nucleus as a region of interest using ImageJ to quantify fluorescence (see also Methods). Measurements were conducted in at least 4 independent experiments for each TF (min 2 experiments for TF alone and 2 experiments for TF fused to VP16 domain). Scale bars: 10 µm. (c,d) Example of results using the *ARF5* reporter plasmid, with (c) and without (d) the VP16 activator domain fused to the TF coding sequence (left and right). Error bars: mean ± s.d; statistical analysis: one-sided Mann-Whitney U-test with $p \leq 0.05$ (*); N of protoplasts (p-values): (c) control, n=35; DOF1.8, n=38 (0.33); KNAT1, n=37 (0.11), LBD3, n=38 (6e-04); SMZ, n= 43 (3e-10); (d) control, n=43 (1e-07); DOF1.8-VP16, n=46; KNAT1-VP16, n=44 (0.37); LBD3-VP16, n=32 (1e-05); SMZ-VP16, n=39 (0.015).

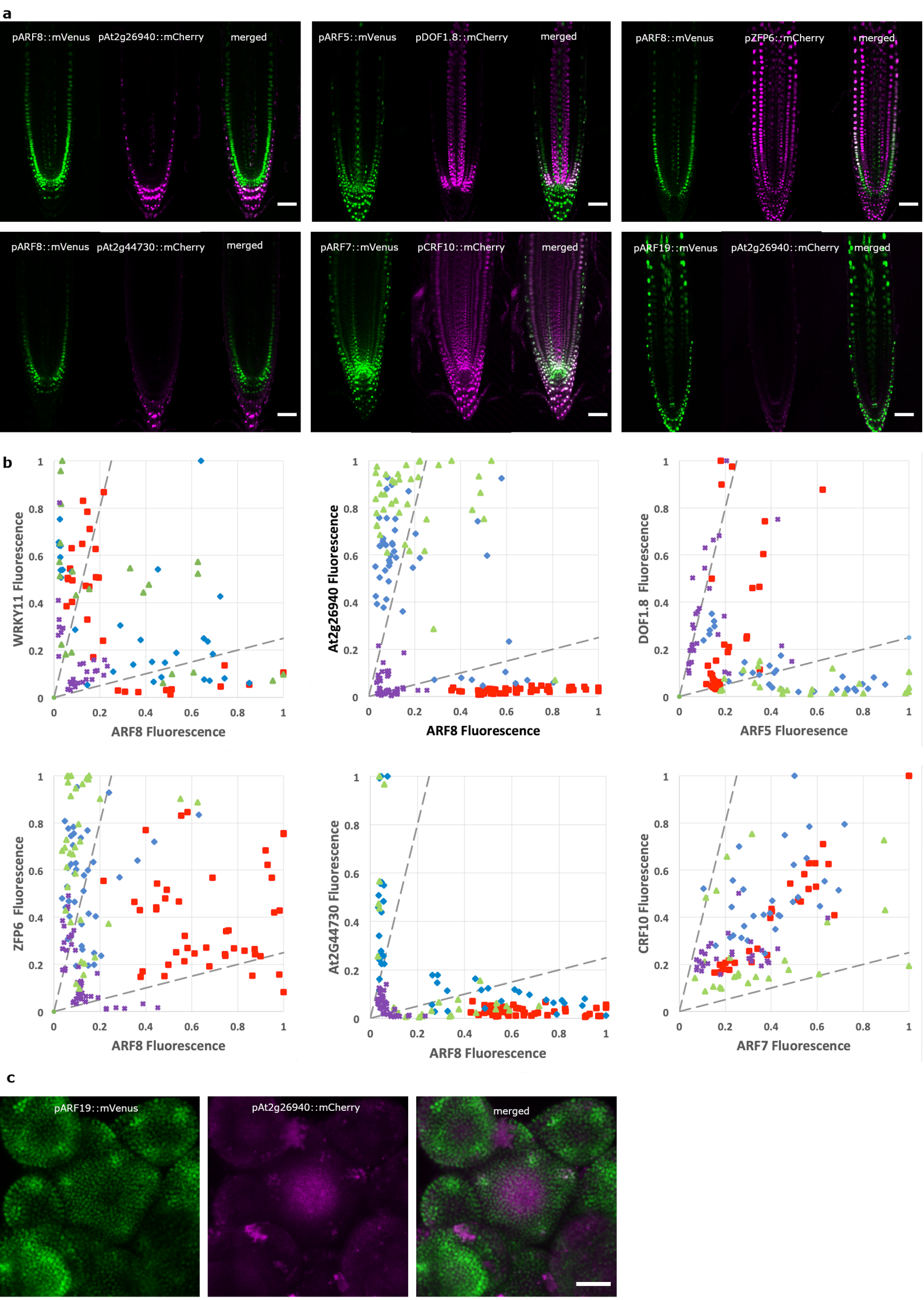
a
pARF8::mVenus pAt2g26940::mCherry merged
pARF5::mVenus pDOF1.8::mCherry merged
pARF8::mVenus pZFP6::mCherry merged
pARF8::mVenus pAt2g44730::mCherry merged
pARF7::mVenus pCRF10::mCherry merged
pARF19::mVenus pAt2g26940::mCherry merged
b
WRKY11 Fluorescence
ARF8 Fluorescence
At2g26940 Fluorescence
ARF8 Fluorescence
DOF1.8 Fluorescence
ARF5 Fluoresence
ZFP6 Fluorescence
ARF8 Fluorescence
At2G44730 Fluorescence
ARF8 Fluorescence
CRF10 Fluorescence
ARF7 Fluorescence
c
pARF19::mVenus
pAt2g26940::mCherry
merged

Extended Data Fig 5. *ARF* transcriptional regulators mostly show complementary expression patterns to their target *ARF*s.

(a) Plants carrying the *ARF* transcriptional reporters were transformed with transcriptional reporters for a subset of *ARF* regulators driving mCherry. For five out of seven constructs (see also Fig.3), we saw complementary patterns of expression between transcriptional repressors and their ARFs in the root. (b) To further quantify the complementarity of TF versus ARF expression, we quantified the red versus green fluorescence levels in individual nuclei from different cell types (root cap = blue diamond, columella = green triangle, epidermis = red square and vascular cells = purple cross). These values were normalized so that the brightest nuclei of each channel in each line was set to 1, and values were plotted onto scatter plots. Any value falling outside the reference lines shows a >4x bias for expression of either TF or ARF (n= 3 for *pAT2G26940::mCherry* and *pAT2G44730::mCherry* in pARF8::mVenus; n= 2 for the remaining genotypes). In some cases there was clear complementarity in some cell types but not others. For example, *ZFP6* shows complementary expression patterns in the root cap, epidermis and columella but overlaps with *ARF8* in the vascular tissues. (c) *At2g26940* expression was also analysed in the SAM where it was found in organ primordia and weakly in the center of the SAM; no clear expression was observed in roots. As previously observed with other developmental and hormonal regulators (22, 23), co-localisation of repressors and their target *ARF* occurs in some cells as in the case of *ZFP6/ARF8* in the root epidermis (a,b) and *At2g26940/ARF19* in shoot organ primordia (c), suggesting potential regulatory interactions to modulate transcription levels. Scale bars: 60 µm (a) and 40 µm (c). Experiments were done two times (a, c).

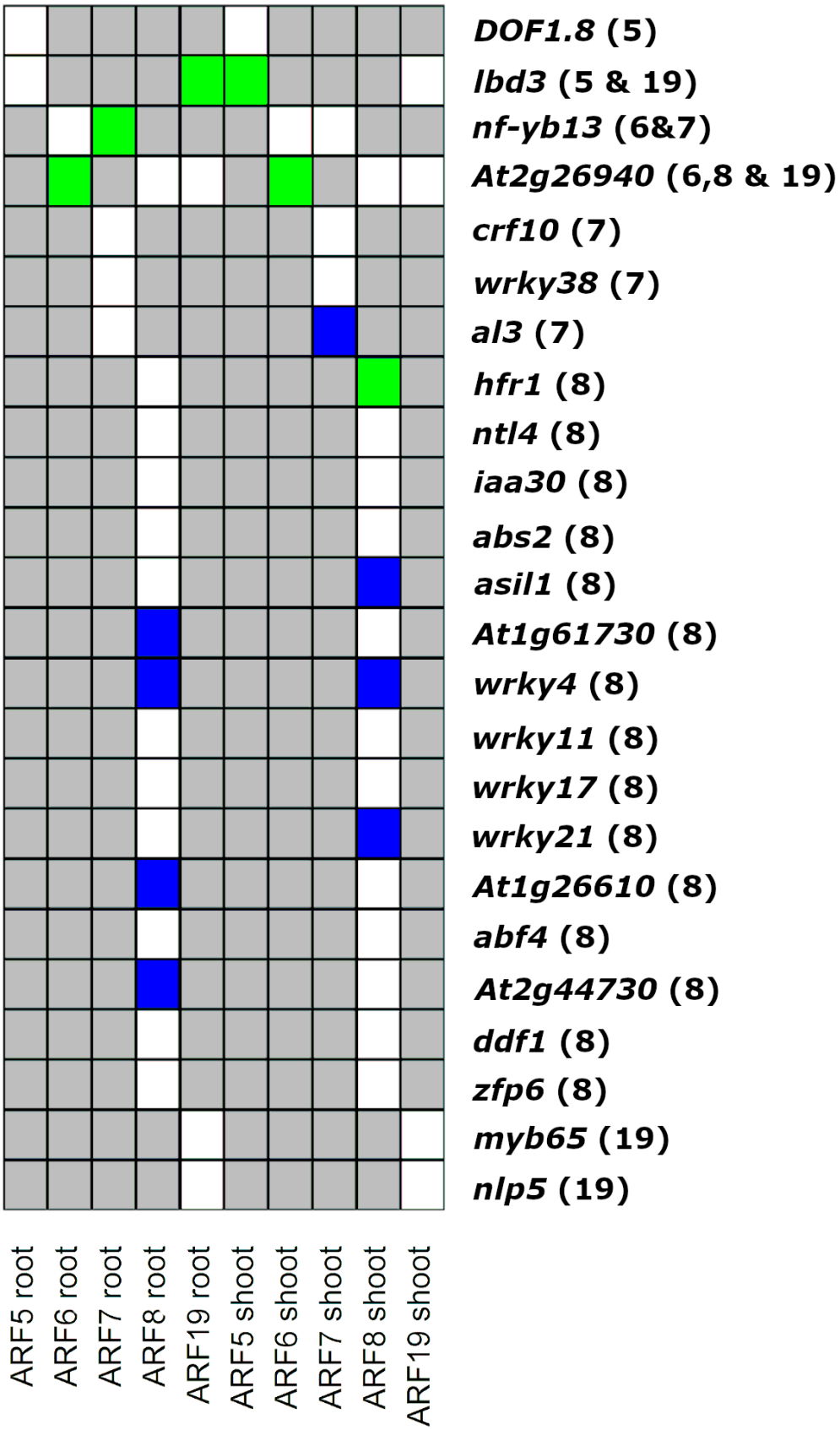
DOF1.8 (5)
lbd3 (5 & 19)
nf-yb13 (6&7)
At2g26940 (6,8 & 19)
crf10 (7)
wrky38 (7)
al3 (7)
hfr1 (8)
ntl4 (8)
iaa30 (8)
abs2 (8)
asil1 (8)
At1g61730 (8)
wrky4 (8)
wrky11 (8)
wrky17 (8)
wrky21 (8)
At1g26610 (8)
abf4 (8)
At2g44730 (8)
ddf1 (8)
zfp6 (8)
myb65 (19)
nlp5 (19)
ARF5 root
ARF6 root
ARF7 root
ARF8 root
ARF19 root
ARF5 shoot
ARF6 shoot
ARF7 shoot
ARF8 shoot
ARF19 shoot

Extended Data Fig 6. Expression of *ARF*^{ClassA} in mutants for the regulatory transcription factors.

Expression of *ARF*^{ClassA} in 24 mutants of the regulatory TFs measured with qRT-PCR, in whole root and whole shoot tissue of 7 days old seedlings. Green boxes indicate statistically significant up-regulation of the corresponding *ARF* in the mutant background compared to wild-type control, and blue boxes indicate statistically significant down-regulation. Statistical analysis was performed using a one-sided Mann-Whitney test and a threshold at $p \leq 0.1$. For simplicity, only the interactions predicted by the Y1H are shown, with other combinations shaded with a grey box. The full data set is available in Supplementary Table 6.

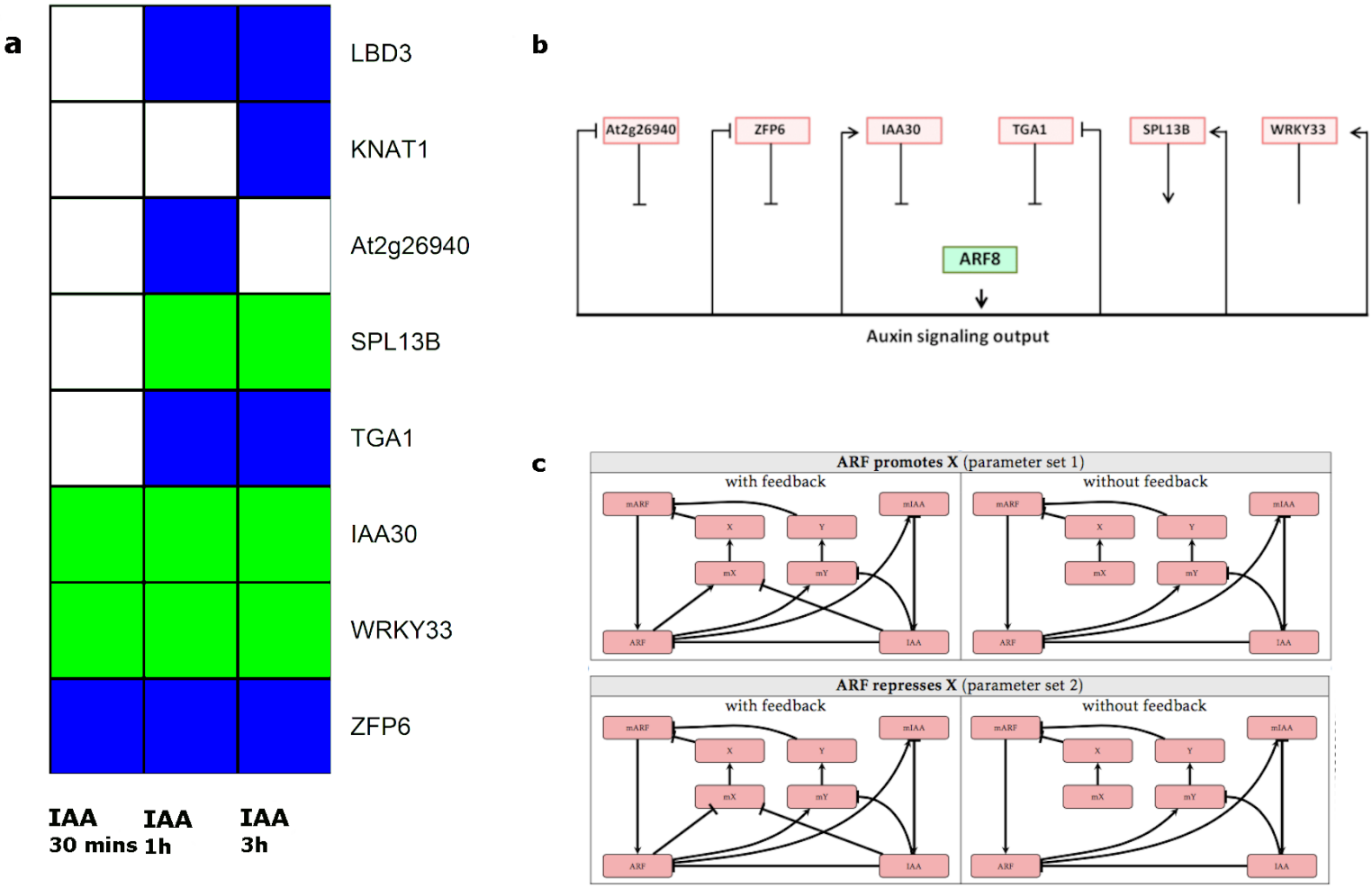
a
LBD3
KNAT1
At2g26940
SPL13B
TGA1
IAA30
WRKY33
ZFP6
IAA 30 mins
IAA 1h
IAA 3h
b
At2g26940
ZFP6
IAA30
TGA1
SPL13B
WRKY33
ARF8
Auxin signaling output
c
ARF promotes X (parameter set 1)
with feedback
without feedback
ARF represses X (parameter set 2)
with feedback
without feedback
mARF
mIAA
X
Y
mX
mY
ARF
IAA
d
Concentration of ARF mRNA. ARF activates X.
Concentration
Simulation including TF Y
Simulation lacking TF Y
Simulation lacking TF Y and without feedback
e
ARF transcription rate. ARF activates X.
SS with TF Y
SS without TF Y
SS without TF Y or feedback
X
Y
f
Concentration of ARF mRNA. ARF represses X.
Concentration
Simulation including TF Y
Simulation lacking TF Y
Simulation lacking TF Y and without feedback
g
ARF transcription rate. ARF represses X
SS with TF Y
SS without TF Y
SS without TF Y or feedback
X
Y

Extended Data Fig 7. Feedback regulations between the transcription factors and auxin signalling.

(a) Expression of several TFs are regulated by auxin, which proves feedback regulation from auxin signaling output primarily on *ARF8* expression. Expression was measured after treatment with 1 μM IAA for 30 min, 1h or 3h (56). Green boxes indicate up-regulation, blue boxes indicate down-regulation of gene expression compared with a mock treatment. (b) Schematic representation of *ARF8* regulation with feedbacks. Feedback from auxin signalling on regulatory TFs is expected to induce complex non-linear regulation of *ARF8* expression (see also Supplementary Note 2). (c) Diagrammatic representation of the interactions taking place for different instances of model analysed in Supplementary Note 2. The two diagrams on the right (without feedback) are identical. However, for comparison with the models with feedback the parameters used for these differ (see Supplementary Note 2). (d-g) On the left: bar chart displaying concentrations before and after knock out of transcription factor X, where Y is activated by ARF (d) or repressed by ARF (f). On the right: Contour plot displaying ARF transcription rate before and after knock out of transcription factor X relative to Y and X populations, where Y is activated by ARF (f), or repressed by ARF (g). Steady state (SS) values corresponding to the bar plot are also reported. These results are discussed in Supplementary Note 2.

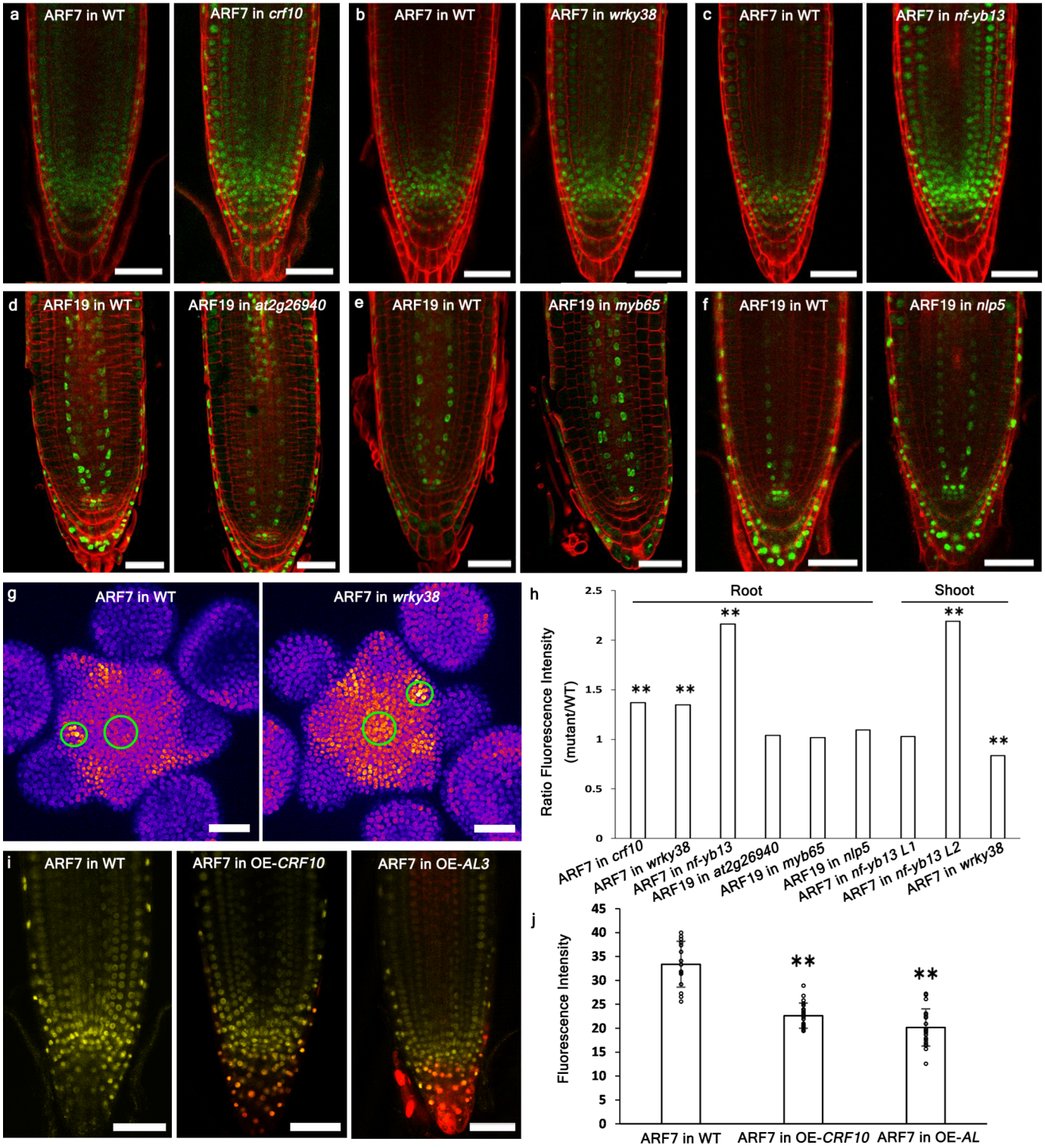
a
ARF7 in WT
ARF7 in crf10
b
ARF7 in WT
ARF7 in wrky38
c
ARF7 in WT
ARF7 in nf-yb13
d
ARF19 in WT
ARF19 in at2g26940
e
ARF19 in WT
ARF19 in myb65
f
ARF19 in WT
ARF19 in nlp5
g
ARF7 in WT
ARF7 in wrky38
h
Root
Shoot
Ratio Fluorescence Intensity (mutant/WT)
2.5
2
1.5
1
0.5
0
**
ARF7 in crf10
ARF7 in wrky38
ARF7 in nf-yb13
ARF19 in at2g26940
ARF19 in myb65
ARF19 in nlp5
ARF7 in nf-yb13 L1
ARF7 in nf-yb13 L2
ARF7 in wrky38
i
ARF7 in WT
ARF7 in OE-CRF10
ARF7 in OE-AL3
j
Fluorescence Intensity
45
40
35
30
25
20
15
10
5
0
**
ARF7 in WT
ARF7 in OE-CRF10
ARF7 in OE-AL

Extended Data Fig 8. Modulating the levels of ARF transcriptional regulators regulates the expression of associated *ARFs*.

(a-f) Comparison of *ARF* expression in wild-type versus mutant in roots. (g) Comparison of *pARF7::VENUS* expression in wild-type versus *wrky38* shoot. For quantification (see (f)), fluorescence was measured in the central zone and primordia 2 (green circles). (h) Quantification of fluorescence changes shown as relative changes in mean fluorescence level in mutant compared to wild-type (single value). Quantifications are shown for (a-g) and for Fig.3c,d. In roots, the total *pARF7/19*-driven fluorescent signal was quantified within a standardized zone covering the stele meristem zone and quantified relative to the wild-type controls. In the shoot, L1 and L2 correspond to quantification in the corresponding layers in the SAM of wild-type and *nf-yb13* (see also Fig.3c,d). Quantification demonstrated a significant change in pattern in *wrky38* mutant SAMs (g), with an increase of *pARF7* activity in the centre and a loss of the differential expression between the SAM centre and lateral organs. Statistical analysis: unpaired two-sided t-test with $p \leq 0.01$ (**). Number of samples observed and quantified: For mutant/wild type roots, 13/13 for *crf10*, 12/14 for *wrky38*, 9/9 for *nf-yb13*, 9/8 for *At2g26940*, 12/11 for *myb65*, 12/10 for *nlp5*; 7 shoots for *nf-yb13* and wild-type controls; 7 shoots for *wrky38* and 6 wild-type controls. P-values from left to right: 0.003, 2e-05, 3e-08, 0.26, 0.57, 0.11, 0.84, 0.007, 0.009. Raw data are provided in Supplementary Table 11. (i) Inducible constitutive overexpression of *CRF10:mCherry* and *AL3:mCherry* in the p*ARF7::VENUS* line. *pARF7::VENUS* is shown in yellow and the transcription factors fused to mCherry in red following a 24h induction with β-estradiol. (j) For both lines shown in (i), we see a significant reduction in *pARF7::VENUS* expression. Unpaired two-sided t-test: p= 4e-10 (*CRF10*) and 2e-10 (*AL3*). Number of plants: wild-type control, n=15; *CRF10*, n=21; *AL3*, n=20. Error bars: mean ± s.d.. Scale bars: 45 µm for root images; 50 µm for shoot images. For each analysis, the confocal settings were identical in the compared genetic backgrounds. All experiments were done two times.

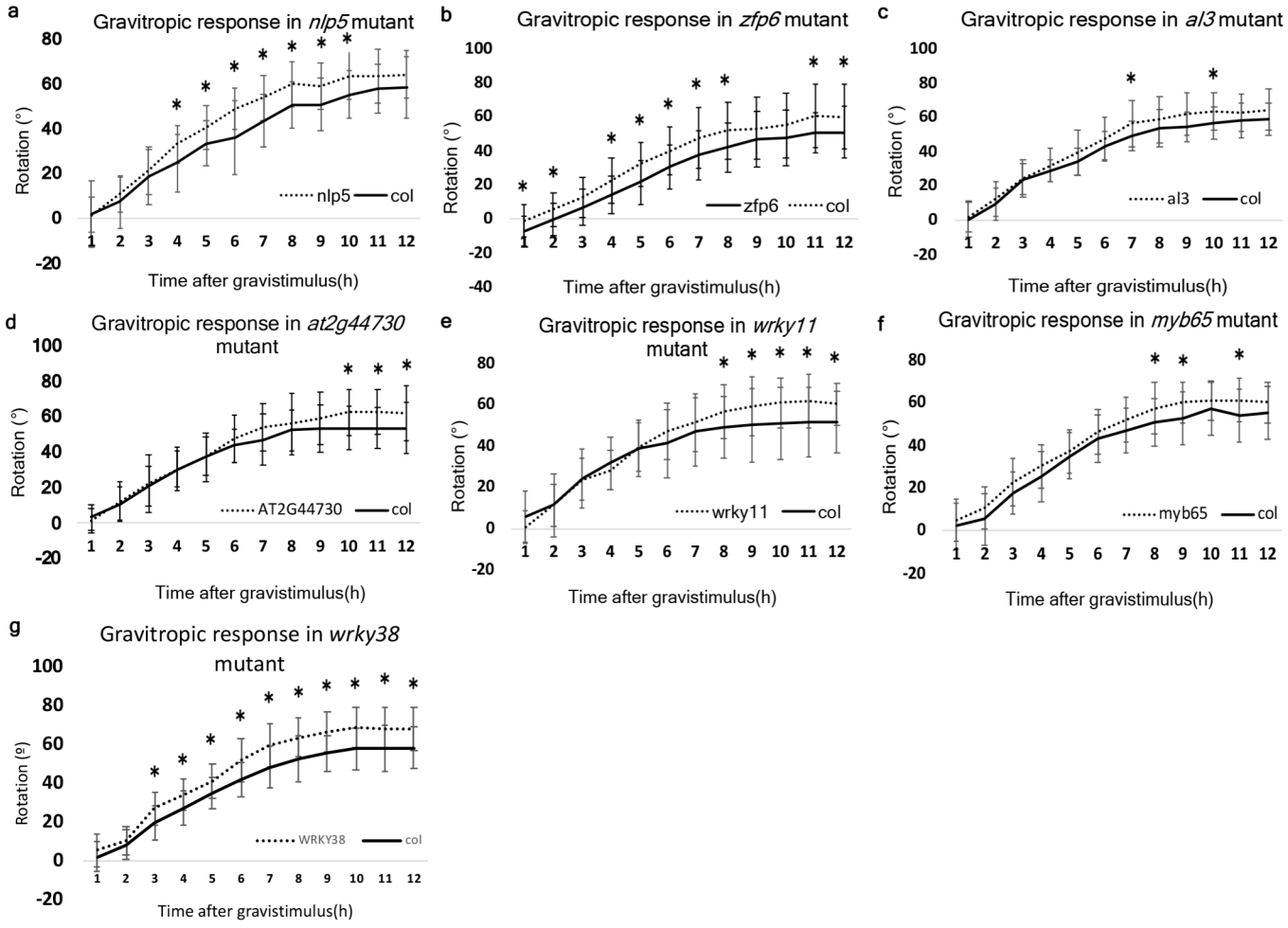
a
Gravitropic response in nlp5 mutant
Rotation (°)
nlp5
col
Time after gravistimulus(h)
b
Gravitropic response in zfp6 mutant
Rotation (°)
zfp6
col
Time after gravistimulus(h)
c
Gravitropic response in al3 mutant
Rotation (°)
al3
col
Time after gravistimulus(h)
d
Gravitropic response in at2g44730 mutant
Rotation (°)
AT2G44730
col
Time after gravistimulus(h)
e
Gravitropic response in wrky11 mutant
Rotation (°)
wrky11
col
Time after gravistimulus(h)
f
Gravitropic response in myb65 mutant
Rotation (°)
myb65
col
Time after gravistimulus(h)
g
Gravitropic response in wrky38 mutant
Rotation (º)
WRKY38
col
Time after gravistimulus(h)

Extended Data Fig 9. Mutations in transcriptional regulators of *ARF*^{classA} accelerate the root gravitropic response.

(a-g) Kinetics of perturbed gravitropic responses of TF mutants (dashed line) compared to wild-type (solid line) over 12h after application of the gravistimulus. Mutants with statistically significant difference in gravitropic response compared to the wild-type are shown: (a) *nlp5*, (b) *zfp6*, (c) *al3*, (d) *at2g44730*, (e) *wrky11*, (f) *myb65* and (g) *wrky38*. Statistical analyses: unpaired two-tailed t-test with $p \leq 0.05$ (*). P-values from 1h to 12h (left to right): (a) 0.86, 0.19, 0.37, 0.004, 0.01, 0.0008, 0.0008, 0.001, 0.007, 0.004, 0.06, 0.07; (b) 0.01, 0.02, 0.05, 0.009, 0.002, 0.007, 0.01, 0.01, 0.14, 0.1, 0.01, 0.04; (c) 0.75, 0.25, 0.85, 0.12, 0.07, 0.16, 0.02, 0.1, 0.01, 0.02, 0.1, 0.06; (d) 0.40, 0.50, 0.71, 0.95, 0.86, 0.23, 0.07, 0.36, 0.12, 0.01, 0.009, 0.04; (e) 0.058, 0.97, 0.88, 0.27, 0.81, 0.16, 0.27, 0.04, 0.03, 0.01, 0.01, 0.01; (f) 0.31, 0.07, 0.09, 0.10, 0.45, 0.26, 0.08, 0.04, 0.01, 0.24, 0.02, 0.11. (g) 0.1, 0.26, 0.003, 0.003, 0.007, 0.0003, 0.0003, 0.0004, 8e-05, 0.0002, 0.001 and 0.001. Sample size (wt/mutant plants): (a) n=29/29, (b) n=32/32, (c) n=28/30, (d) n=28/26, (e) n=30/29, (f) n=30/28, (g) 29/30. Raw data are provided in Supplementary Table 12. Error bars: mean ± s.d..

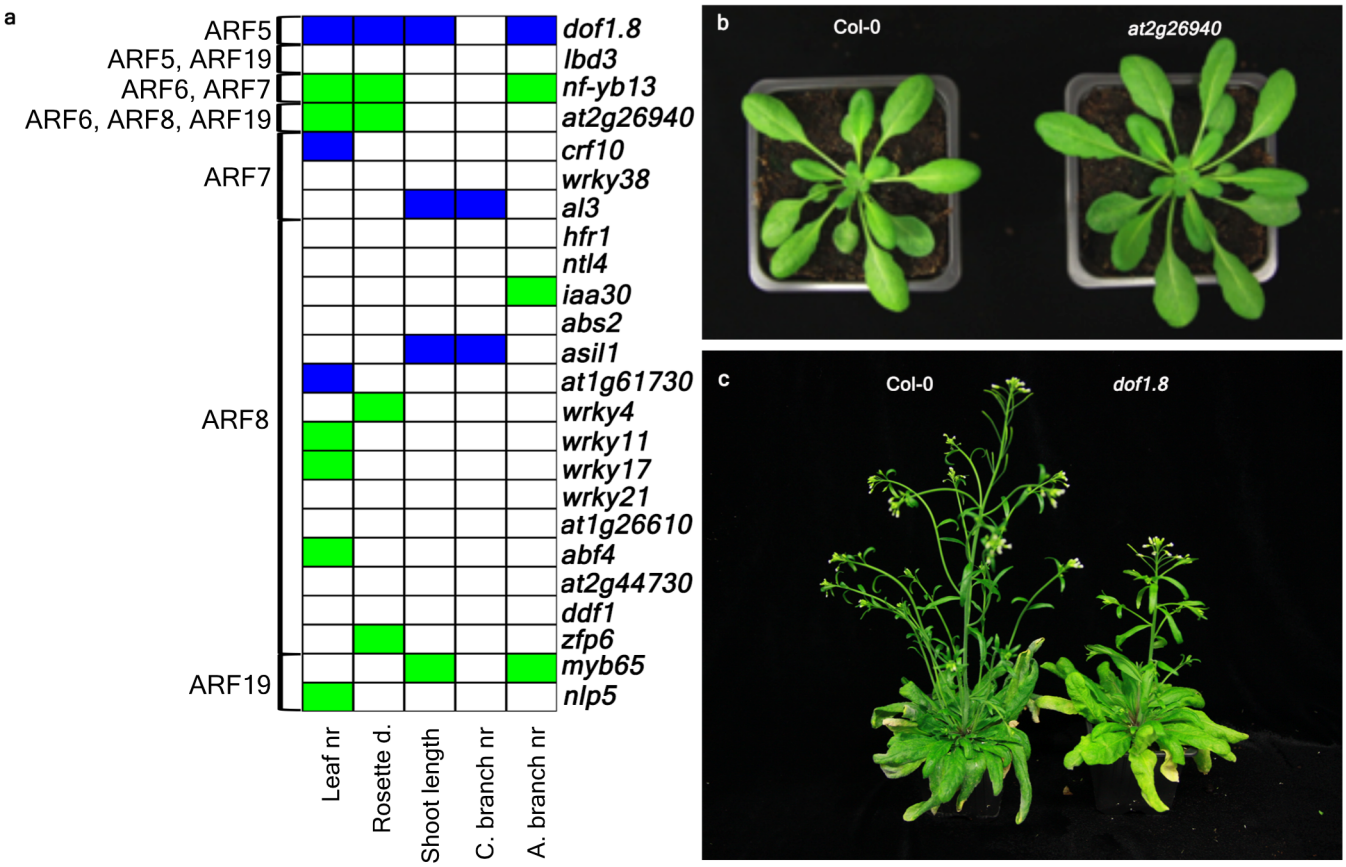
a
ARF5
ARF5, ARF19
ARF6, ARF7
ARF6, ARF8, ARF19
ARF7
ARF8
ARF19
dof1.8
lbd3
nf-yb13
at2g26940
crf10
wrky38
al3
hfr1
ntl4
iaa30
abs2
asil1
at1g61730
wrky4
wrky11
wrky17
wrky21
at1g26610
abf4
at2g44730
ddf1
zfp6
myb65
nlp5
Leaf nr
Rosette d.
Shoot length
C. branch nr
A. branch nr
b
Col-0
at2g26940
c
Col-0
dof1.8

Extended Data Fig 10. Transcriptional regulation of *ARF*^{classA} regulates shoot development.

(a) Phenotypic analysis of the shoot defects in TF mutants. Leaf nr: leaf number; Rosette d.: Rosette diameter; C. branch nr: cauline branch number; A. branch nr: axillary branch number. Green boxes indicate statistically significant increases, blue boxes indicate statistically significant reductions in the indicated developmental parameter compared to Col-0. Statistical analyses: unpaired two-tailed t-test, $p \leq 0.05$ considered as statistically significant; number of plants n=12 per genotype. (b) Examples of shoot growth phenotypes: shoot growth during vegetative stage in the *at2g26940* mutant alongside the control after growth for 43 days in short day conditions. (c) The *dof1.8* mutant flowers earlier than control plants.